Dissolution of cations in C-(N,K-)A-S-H gels at the nanoscale

Liu, Chen; Tao, Yong; Nie, Shuai; Chen, Yun; Li, Zhenming; Poon, Chi Sun; Ye, Guang

DOI
10.1016/j.compositesb.2025.112337

Publication date
2025

Document Version
Final published version

Published in
Composites Part B: Engineering

Citation (APA)
Liu, C., Tao, Y., Nie, S., Chen, Y., Li, Z., Poon, C. S., & Ye, G. (2025). Dissolution of cations in C-(N,K-)A-S-H gels at the nanoscale. *Composites Part B: Engineering*, *297*, Article 112337. https://doi.org/10.1016/j.compositesb.2025.112337

Composites Part B 297 (2025) 112337

Contents lists available at ScienceDirect

Composites Part B

journal homepage: www.elsevier.com/locate/compositesb

Dissolution of cations in C-(N,K-)A-S-H gels at the nanoscale

Chen Liu [a,1], Yong Tao [b,1], Shuai Nie [c], Yun Chen [a,d], Zhenming Li [e,f,*], Chi Sun Poon [b], Guang Ye [a,**]

[a] Department of Materials and Environment (Microlab), Faculty of Civil Engineering and Geoscience, Delft University of Technology, 2628, CN Delft, the Netherlands
[b] Department of Civil and Environmental Engineering & Research Centre for Resources Engineering Towards Carbon Neutrality, The Hong Kong Polytechnic University, Hung Hom, Kowloon, Hong Kong
[c] Department of Chemistry and Bioscience, Aalborg University, Aalborg DK-9220, Denmark
[d] School of Materials Science and Engineering, South China University of Technology, 510006, Guangzhou, Guangdong, China
[e] School of Civil and Environmental Engineering, Harbin Institute of Technology, 518000, Shenzhen, China
[f] Guangdong Provincial Key Laboratory of Intelligent and Resilient Structures for Civil Engineering, Harbin Institute of Technology, 518000, Shenzhen, China

ARTICLE INFO

Handling Editor: Uday Vaidya

Keywords:
C-(N,K-)A-S-H gels
Leaching
^{23}Na MAS NMR
Molecular dynamics simulation
Thermodynamics
Dissolution free energy

ABSTRACT

Alkali and alkali earth metal ions are normally present in the gels of alkali-activated materials as well as blended PC-based materials. Previous studies have revealed that the leaching of these cations can trigger the change in gel structure and even the gel decomposition. However, the dissolution of cations was rarely known and the underlying mechanisms remained unclear. To address this issue, five calcium-(sodium, potassium-)aluminum-silicate hydrates (C-(N,K-)A-S-H gels) with different Ca/Si ratios (0.8–1.2) and Al/Si ratios (0.1–0.3) were synthesized to investigate the leaching behaviour of Ca, Na and K. For the first time, the dissolution free energies of Ca, Na and K in C-(N,K-)A-S-H gels were calculated using molecular dynamics simulations with the metadynamics method. Experimental results showed that Na showed the highest leaching ratio, followed by K and Ca, attributed to the lowest dissolution free energy of Na. The gel with a higher Ca/Si ratio or a lower Al/Si ratio showed higher charge positivity on the surface, resulting in reduced leaching of the three cations. Additionally, the presence of K was found to promote the dissolution of Na in gels.

1. Introduction

Calcium-silicate-hydrate (C-S-H) gels serve as the foundational hydration products within cementitious materials, which play a pivotal role in the mechanical properties and durability of concrete structures [1]. Calcium-(aluminium-)silicate-hydrate (C-(A-)S–H) gels, emerging as variants to the conventional C-S-H gels, tend to form in hardened cement systems with the integration of some Al-rich supplementary cementitious materials (SCMs) such as fly ash and calcined clay [2]. The strategic incorporation of SCMs is of great importance in concrete technology. This approach not only facilitates the consumption of excess portlandite, resulting in a denser microstructure but also decreases the demand for cement. Consequently, it can reduce the carbon footprint in the concrete industry and aligns with global initiatives towards achieving net-zero emissions. To this end, an increasing number of solid waste materials have been utilized as binders, with some natural pozzolans containing a large portion of bound alkalis [3]. This not only results in an increased pH in the pore solution but also promotes the uptake of alkalis by gels. Alternatively, in formulations with lower cement content or even in cement-free binders, researchers employ alkali activators instead of water to enhance the reactivity of SCMs (or precursors), successfully producing sustainable construction materials known as “alkali-activated materials” (AAMs) or geopolymer [4]. Most of these materials have been proven to efficiently lower carbonation emissions in building sections [5].

Due to the high reactivity of Ca-rich precursor and free of high-temperature curing, slag blended AAMs, also known as alkali-activated slag (AAS), have garnered significant interest in both academic research and engineering practice. C-(N,K-)A-S-H gels are the primary reaction products in AAS systems. Compared with the C-(A-)S–H gel in PC-based systems, C-(N,K-)A-S-H gels show lower Ca/(Si + Al) ratios (0.6–1.2) and higher Al/Si ratios (0.1–0.3) [6,7], resulting in a

* Corresponding author. School of Civil and Environmental Engineering, Harbin Institute of Technology, 518000, Shenzhen, China.
** Corresponding author.
E-mail addresses: c.liu-12@tudelft.nl (C. Liu), zhenmingli@hit.edu.cn (Z. Li), G.Ye@tudelft.nl (G. Ye).
[1] These authors contributed equally to this work.

https://doi.org/10.1016/j.compositesb.2025.112337
Received 25 July 2024; Received in revised form 17 February 2025; Accepted 23 February 2025
Available online 25 February 2025

more cross-linked structure (primarily Q^2, with some Q^1 and Q^3) [8,9]. Moreover, it is noteworthy that not only Ca ions but also alkali metal ions like Na and K ions can be intercalated into the interlayer of C-(N,K-)A-S-H gels, effectively compensating for the negative charges induced by the high Al substitution for Si [10,11].

To eliminate the interference of other phases in pastes or concrete, researchers have employed synthetic gels to study their chemical and physical properties. Myers et al. [11] investigated the relationship between the structure and chemical composition of C-(N,K-)A-S-H gels under equilibrium at 50 °C. The gels synthesized using alkaline hydroxide solutions exhibited increased basal spacing with lower Ca and higher alkali contents, while Al content showed a limited impact. Garcia-Lodeiro et al. [12] studied the compatibility between synthetic C-A-S-H gels and N-A-S-H gels. In the presence of Ca, N-A-S-H gels remained stable only at a pH below 12. Beyond this range, Ca began to disrupt the three-dimensional structure of N-A-S-H gels, leading to the formation of C-(N-)A-S-H gels. Wang et al. [13] explored the degradation of synthetic C-(N-)A-S-H and N-A-S-H gels exposed to sulfuric acid solutions. Both types of gels showed a higher degree of polymerization upon exposure. In addition, dealumination and decalcification in the C-(N-)A-S-H gels were observed, along with a considerable and rapid loss of Na and a minor loss of Si. Liu et al. [14] investigated the structural change in synthetic C-(N-)A-S-H gels under water immersion and found that the leaching of Na triggered the structural change of C-(N-)A-S-H gels. The charge-compensating role of the leached Na in the interlayer was taken over by intralayer Ca, resulting in the decalcification of silicate chains and the formation of a more crosslinked gel structure.

In addition to experimental characterizations, atomic simulations including density functional theory (DFT), molecular dynamics (MD) simulation and Grand Canonical Monte Carlo (GCMC) simulation are powerful strategies for probing the intricate details of gel atomic structure, intrinsic mechanical properties and chemical resistance of the gels [15,16]. However, most studies focus on C-(A-)S-H gels. Qomi et al. [17] theoretically confirmed the affinity of Al-Si substitution at the bridging site of silicate chains. In addition, the replacement of interlayer Ca with Al has been identified as a healing process, leading to the formation of $[AlO_5]$ and $[AlO_6]$ species. These substitutions contributed to an increased mean silicate chain length, enhanced cross-linkage between layers and improved mechanical properties. Churakov et al. [18] found that the chemical affinity of Al within C-S-H gels was influenced by both electrostatic interactions and the molar ratio of $Al(OH)_4^-/SiO(OH)_3^-$. The most pronounced affinity for Al occurred at pH∼11.5, which corresponded to the maximum concentration of $SiO(OH)_3^-$. Hou et al. [19–21] delved into the transport of water and ions within the nanopore of C-(A-)S-H gels (Ca/Si = 0.75 and Al/Si = 0–0.2). Their findings indicated that the presence of Al at the surface of C-(A-)S-H gels heightened the electronegativity of the solid oxygen atoms. Consequently, this polarization intensified the dipole moment of surface water molecules, reinforcing the interfacial hydrogen bonding and prolonging the residence time of water near the aluminate substrate. In a recent publication [22], Tao et al. revealed the accelerated decalcification mechanism of C-S-H gels exposed to seawater using the metadynamics simulation method. The "ion exchange" between surface Ca and electrical double layers significantly reduced the dissolution free energy of Ca in seawater.

Previous experimental and computational investigations have shown that limited research has concentrated on the leaching behaviours of cations in C-(N,K-)A-S-H gels, especially concerning alkali metal ions. The inclusion of alkali metal ions is one of the most distinguishing characteristics of C-(N,K-)A-S-H gels compared to C-(A-)S-H gels. According to [11,13,14], the leaching amount of alkali metal ions in C-(N,K-)A-S-H gels was considerably higher than that of other ions, which presented specific challenges for AAS materials. On one hand, the leaching of alkali metal ions can alter the gel structure [14], potentially leading to gel decomposition and reduced mechanical properties of AAS materials after long-term water immersion [23–25]. On the other hand, efflorescence, characterized by the appearance of white deposits on or beneath the surface of materials [26], presents both cosmetic and structural problems for AAMs [27]. The formation of efflorescence has been directly related to the leaching of alkali metal ions [28]. Finally, the leaching stability of K in gels has been scarcely involved in the existing literature. Gaining insight into this issue would enhance our comprehension of the binding stability of K with gels and how it differs from that of Na. To sum up, it is of great importance to understand the dissolution of cations in C-(N,K-)A-S-H gels.

In this study, five C-(N,K-)A-S-H gels were synthesized with different Ca/Si ratios (0.8 and 1.2), Al/Si ratios (0.1 and 0.3) and alkali types (Na and K), representing the typical compositions of gels in AAS systems. We measured the ion concentration in the leachate of gels subjected to deionized water immersion with time and quantified the leaching ratio of cations from the gels. Solid-state ^{23}Na magic angle spinning (MAS) nuclear magnetic resonance (NMR) was performed to explore the coordination condition and mobility of Na within the gels. Additionally, C-(N,K-)A-S-H gel models were constructed by cleaving the gel structure along the interlayers to form 5 nm slit pores. The dissolution free energies of Ca, Na and K ions from different gel surfaces were calculated using MD simulations with the metadynamics method. Then, scattered alkali hydroxide molecules were randomly introduced into the nanopore to study the atomic density and the diffusion coefficient of cations at different distances from the gel substrates. We hope the insights of this work can provide compelling knowledge to better understand the dissolution behaviours of cations within C-(N,K-)A-S-H gels.

2. Experiments

2.1. Gel synthesis

The sol-gel method has garnered increasing interest in recent years due to its repeatability, controllability, and efficiency. In this work, the gels were synthesized through this method as described in [14]. The synthetic gels were classified into two types based on the presence or absence of K: C-(N-)A-S-H gels and C-(N,K-)A-S-H gels. For the C-(N-)A-S-H gels, a 0.6 M Na_2SiO_3 solution, a 0.12 M $Al(NO_3)_3$ solution, and a 0.24 M $Ca(NO_3)_2$ solution were prepared using analytical reagent (AR) chemicals and deionized water to serve as the sources of Si, Al, and Ca, respectively. A 10 M NaOH solution was used to maintain the pH above 14, which was similar to the pH of the pore solution in normal AAS systems [23]. For the C-(N,K-)A-S-H gels, the sources of Si, Al and Ca were identical to those mentioned above, while K was supplied by a 10 M KOH solution that also served to adjust the pH.

The proportions of chemical solutions are detailed in Table 1. For all gels with a target Ca/Si ratio of 0.8, the molar Ca/Si ratio calculated from the precursor solutions was lower than 0.8 due to the high solubility of Si and Al and the relatively low solubility of Ca under strong alkaline conditions [14]. The gels were labelled using the format "target Ca/Si ratio_target Al/Si ratio_target percentage of alkali metal ions". For instance, "0.8_0.3_50Na50K" indicated a gel with a Ca/Si ratio of 0.8, an Al/Si ratio of 0.3, and a Na/K ratio of 50/50. The Ca/Si (0.8 and 1.2) and Al/Si (0.1 and 0.3) ratios were tailored to cover the common range of elemental ratios in AAS systems [23]. The gels labelled "0.8_0.1_100Na", "0.8_0.3_100Na" and "1.2_0.3_100Na" were used to study the impact of varying elemental ratios on the dissolution behaviour of cations, while

Table 1
Component of chemical solutions for gel synthesis (unit: ml).

	Na_2SiO_3	$Ca(NO_3)_2$	$Al(NO_3)_3$	NaOH	KOH	H_2O
0.8_0.1_100Na	80	100	40	50	–	80
0.8_0.3_100Na	80	100	120	50	–	–
0.8_0.3_50Na50K	80	100	120	25	25	–
0.8_0.3_10Na90K	80	100	120	0	50	–
1.2_0.3_100Na	50	150	75	50	–	25

the gels labelled "0.8_0.3_100Na", "0.8_0.3_50Na50K" and "0.8_0.3_10Na90K" were employed to specifically investigate the dissolution behaviour of Na and K ions.

In a glove box with N_2 atmosphere, the solutions were meticulously introduced dropwise into a conical flask in the following order: NaOH/KOH, Na_2SiO_3, $Al(NO_3)_3$, $Ca(NO_3)_2$ solutions and deionized water [29]. The solutions were continuously stirred by magnetic stirrers within the airtight conical flasks. After 7 d of reaction, the resulting fresh solid was centrifugated, collected and washed. The cleaning process involved an ultrasonic bath using deionized water three times and absolute ethanol once, with each treatment lasting 2 min, to remove ions adhered to the gel [30]. The washed gel was then dried in a vacuum freeze dryer until a constant weight was achieved. Subsequently, the dried gel was carefully stored in a desiccator, where a RH of 30 % was maintained by a saturated $CaCl_2$ solution [31].

The chemical composition of gels measured by X-ray fluorescence (XRF), along with the calculated atomic ratios of synthetic gels are presented in Table 2. The obtained atomic ratios of gels closely aligned with the designated values. A comparison among the 0.8_0.3_100Na, 0.8_0.3_50Na50K and 0.8_0.3_10Na90K gels revealed that a higher K content resulted in lower contents of Ca and Na. This was probably due to the competition among Ca, K and Na ions in gels. The phase assemblage of the synthetic gels was identified by XRD using a Bruker D8 Advance diffractometer with CuKα radiation (1.54 Å), a step size of 0.02° and a dwell time of 5 s per step.

2.2. Leaching test

In order to monitor the leaching behaviour of the gels, around 0.500 g (± 0.005 g) of gels were immersed in 100 ml of deionized water within a polyethene bottle at 20 °C. The bottle was shaken every 10 min for the first hour and then every 30 min from 1 h to 6h. After 5 min, 10 min, 30 min, 1 h, 3 h, and 6 h of water immersion, the leachate was extracted using a 0.22 μm syringe-driven filter by Millex®, respectively. The ion concentration of Si, Al, Ca, Na, and K in the obtained leachate was measured using a PerkinElmer Optima 5300DV ICP-OES spectrometer. All samples were diluted and acidified using nitric acid (0.2 vol%). For each sample, ion concentrations were measured in duplicate, and we used the average of these two measurements as the final result. If the deviation between the two measurements exceeded 10 %, a third measurement was performed.

The "leaching amount" of ions from gels can be directly determined through ICP results. However, to calculate the "leaching ratio", the "total amount" of each ion in the gel needed to be determined first. Around 0.100 g (± 0.005 g) of synthetic gels were dissolved into 100 ml of 0.1 M HCl solution at 20 °C [32]. Upon the complete dissolution of the solid phase, the leachate was collected and ion concentration was measured by ICP-OES. Finally, the "leaching ratio" of ions could be calculated as the "leaching amount"/"total amount", which can be regarded as the "leaching potential" of ions. The term "leaching potential" refers to the ability of a substance to migrate from solid materials into liquid media. This concept has been widely used in studies on the leaching of heavy metal ions from solid waste and soil [33–35]. In other words, a higher leaching ratio indicates a higher leaching potential of ions.

2.3. ^{23}Na MAS NMR

^{23}Na MAS NMR spectroscopy was utilized to probe the local chemical environments of Na and to quantify the Na contents present in the synthetic C-(N,K-)A-S-H gels. The ^{23}Na MAS NMR spectra were performed on a Bruker Avance NMR spectrometer operating at a magnetic field strength of 14.1 T, using a triple-resonance ^{1}H-X-Y 2.5 mm Bruker CP/MAS probe, with a spinning frequency of $\nu_R = 25.0$ kHz. Since ^{23}Na is a quadrupolar nucleus, a short excitation pulse (0.5 μs, corresponding to ~11° with an rf field strength of $\gamma B_1/2\pi = 60$ kHz) was used for the reliable quantitative evaluation of ^{23}Na sites experiencing different quadrupolar couplings. In addition, the intensity of each spectrum was corrected with the weight of the sample packed in the rotor. Typically, each measurement comprised 4096 scans with a relaxation delay of 2 s. The isotropic chemical shifts were referenced to external samples of a 1.0 M NaCl solution.

3. MD simulations

3.1. Model construction

The above experiments revealed the leaching behaviours of ions within different gels, while MD simulations contributed to elucidating the underlying mechanisms. In C-(N,K-)A-S-H gels, Na and K ions typically exhibit similar behaviour to Ca ions, while Al and Si ions serve as anionic groups (*i.e.*, [AlO_{4-6}] and [SiO_4]) for charge balance [36]. In this regard, the equivalent Ca/Si ratio of C-(N,K-)A-S-H was estimated by the (Ca + Na + K)/(Al + Si) ratio. This value for synthetic samples was similar to (slightly higher than) the Ca/Si ratio of the 14 Å tobermorite, thereby making the 14 Å tobermorite a suitable prototype for constructing the amorphous molecular models of C-(N,K-)A-S-H gels. The model construction procedure is demonstrated in Fig. 1. First, the orthorhombic unit cell (Fig. 1B) was constructed by redefining the lattice vectors of an original monoclinic unit cell of 14 Å tobermorite (Fig. 1A) obtained from the literature [37]. Then, the orthorhombic unit cell was duplicated into a 2 × 4 × 1 supercell of C-S-H gels (Fig. 1C). The bridging [SiO_4] groups were partly removed or replaced by [AlO_4] groups to align with the Ca/Si and Al/Si ratios of the C-(N-)A-S-H gels in Table 2. Na ions were inserted into the interlayers to achieve the desired Na/Si ratios and to neutralize the net negative charges engendered by the substitution of Al ions for Si ions (Fig. 1D). However, based on the experimentally measured atomic ratios of Si, Al, and Na (Table 2), the number of introduced Na ions was insufficient to fully compensate for the charge imbalance caused by Al substituting for Si. Hence, additional H^+ or OH^- were introduced into the structures for final charge balancing. For C-(N,K-)A-S-H models, Na ions were partly substituted by K ions to meet the compositions of synthetic gels.

All the developed C-(N-)A-S-H and C-(N,K-)A-S-H models went through a comprehensive annealing process utilizing a reactive force field [38] to ensure the structural stability before their use in constructing the surface models for cation dissolution (section 3.2) and diffusion (section 3.3) calculations. During the annealing process (Fig. 1E), the system was heated from 300 K to 500 K in 500 ps and equilibrated at 500 K for 1000 ps. Then it was cooled to 300 K in 500 ps and equilibrated at 300 K for 1000 ps. The whole process was conducted under the isothermal-isobaric (NPT) ensemble with a time step of 0.2 fs.

Table 2
Chemical compositions (wt.%) and elemental ratios of the synthetic gels.

	CaO	SiO_2	Al_2O_3	Na_2O	K_2O	Ca/Si	Ca/(Si + Al)	Al/Si	Na/Si	K/Si
0.8_0.1_100Na	40.63	50.89	3.67	4.71	–	0.85	0.78	0.09	0.18	–
0.8_0.3_100Na	38.32	46.06	8.50	7.12	–	0.89	0.74	0.21	0.29	–
0.8_0.3_50Na50K	35.66	48.28	9.21	2.77	4.08	0.79	0.65	0.22	0.11	0.11
0.8_0.3_10Na90K	32.86	48.35	9.80	0.76	8.23	0.73	0.60	0.23	0.03	0.22
1.2_0.3_100Na	49.12	41.38	7.54	1.96	–	1.27	1.05	0.21	0.09	–

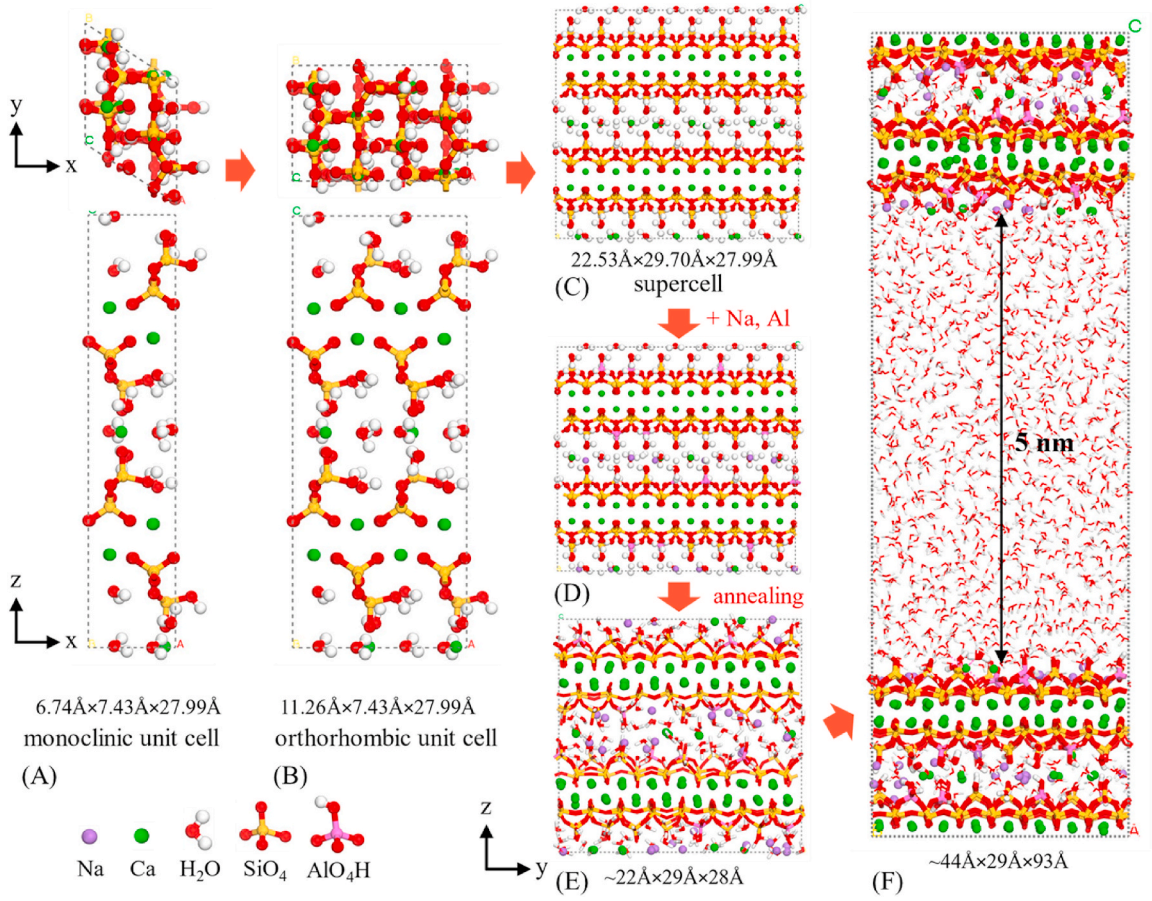

Fig. 1. Schematic demonstration of the model construction procedure, taking the "0.8_0.1_100Na" model as an example.

The annealing scheme for accelerating the protonation of cement minerals has been widely adopted in previous studies [38,39]. The "nanopore model" was widely used to investigate the dissolution and diffusion of ions in gels [15,22], which was constructed by cleaving the gel structure at the interlayer (Fig. 1F). The surface models were constructed by cleaving the C-(N,K-)A-S-H structure at the interlayer. According to the nanoscale C-S-H model [40], the gel pore of C-S-H was about 2–5 nm. Since our study focused on ion transport, a larger gel pore was necessary to increase the transport space and sample ions, ensuring the accuracy of the modelling. Therefore, we produced a 5 nm slit pore between the gel substrates and saturated it with water (Fig. 1F). Three different C-(N-)A-S-H nanopore models are presented in Fig. 2. All C-(N,K-)A-S-H gel models have similar dimensions, approximately 45 Å × 30 Å × 95 Å, with a total atom count of around 11,600. All MD simulations were carried out using the LAMMPS software [41].

3.2. Dissolution free energy calculations

Dissolution free energy measures the energy change when a solute dissolves in a solvent, essential for predicting solubility and designing materials. Dissolution free energy is the most important quantity that bridges dissolution thermodynamics and kinetics [42]. However, the calculation of free energy from standard MD simulations is infeasible, because the ion dissolution process usually takes more than microseconds to be observed while MD simulations typically have a time limit of a few nanoseconds. Therefore, advanced sampling methods such as metadynamics [43], umbrella sampling [44], steered MD [45], *etc.* have been developed to enhance the sampling of configuration space within affordable computational cost. In particular, metadynamics has the advantage of no requirement for predefined reaction pathways, making it a desirable candidate for simulating complicated processes like dissolution where the exact dissolution pathway is unknown before.

To understand the intrinsic leaching properties of Na, K, and Ca ions in the C-(N,K-)A-S-H gel, we calculated the dissolution free energy of C-(N,K-)A-S-H gels. The calculation was implemented by a well-tempered metadynamics method [46,47] with the external library Plumed [48] patched in LAMMPS. The dissolution free energy barrier was typically determined by the breaking and formation of chemical bonds within 5 Å of the surface. Using a larger dissolution distance cutoff did not significantly affect the accuracy of the free energy calculations but would substantially increase the computational load. Therefore, we calculated the free energy landscape of cations within 12 Å above the surface, which was a very safe cutoff. Based on our previous experience in the Ca ion dissolution simulation of belite [49] and C-S-H gels [22], three collective variables (CVs) of displacement components of target Na, K, and Ca ions in x, y, and z directions were used as the biasing CVs while an additional CV of the coordination number of target ions with surface oxygen (*i.e.*, number of surface restraints) was calculated as an observation CV during the metadynamics simulation. To eliminate the influence of the initial configuration on the ion dissolution, we have chosen four representative sites for each type of cation to calculate the dissolution free energy, as presented in Fig. 3. All selected sites shared a close number of surface restraints around 3, which was a typical value of a kink or step site in the classical Terrace-Ledge-Kink model [50,51]. The well-tempered metadynamics used the biasing potential of Gaussians with a width of 0.1 Å and added frequency of every 200 timesteps. The initial height of Gaussian potentials was 1.5 kJ/mol and changed by a bias factor of 10 during the well-tempered metadynamics sampling to obtain better convergence. The free energy calculations were performed under the NVT ensemble using a reactive force field with a time step of

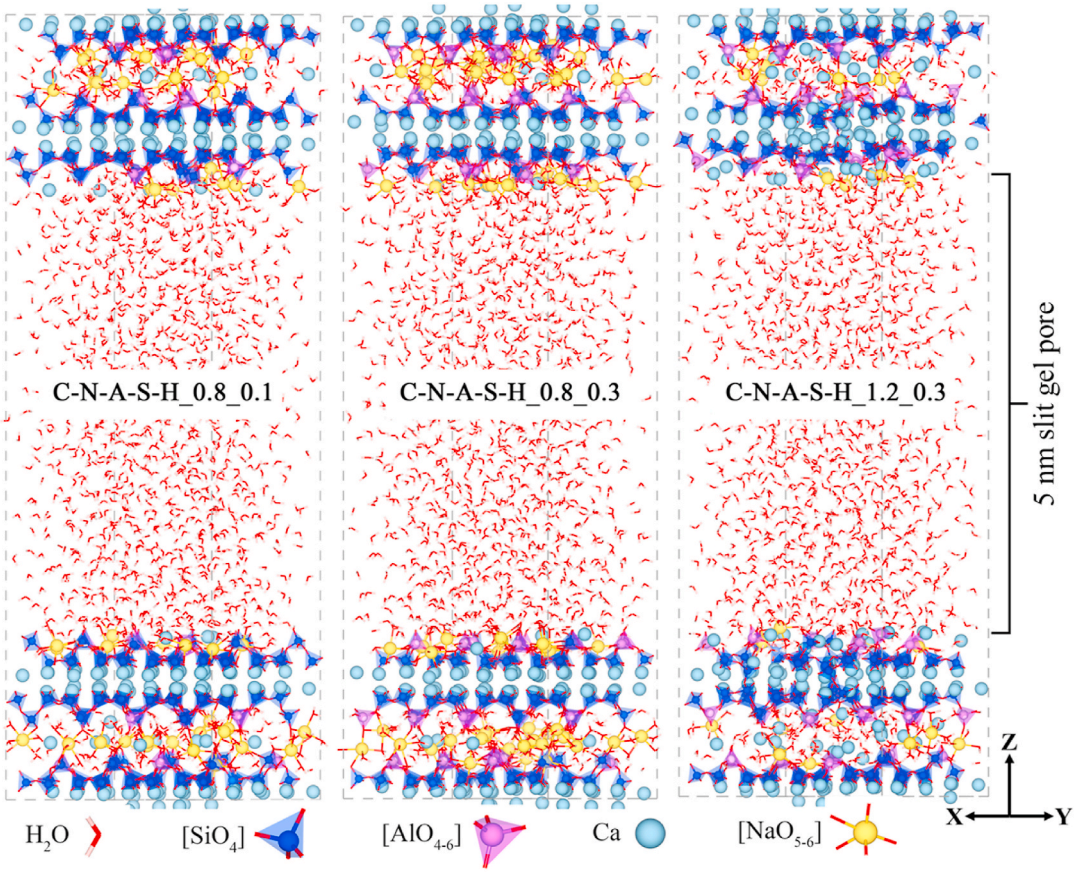

Fig. 2. Schematic representation of nanopore models of three C-(N-)A-S-H gels. "0.8" and "1.2" refer to Ca/Si ratios, while "0.1" and "0.3" denote the Al/Si ratios. To clearly illustrate the entire gel structure, the gel model is rotated 45° along the z-axis. A more detailed view of the gel structure at the ab plane is shown in Fig. 3.

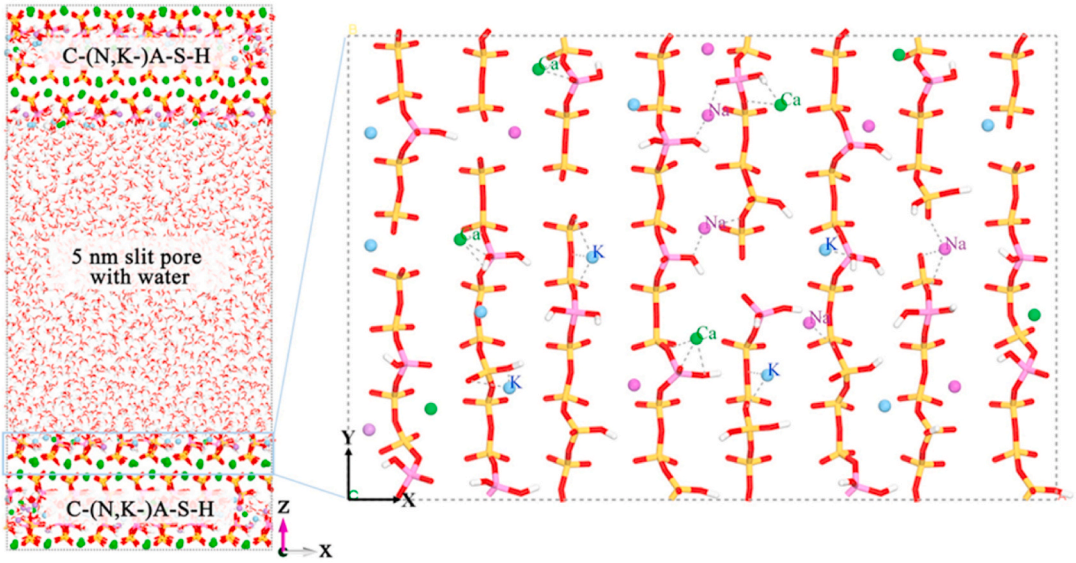

Fig. 3. Atom arrangement of the disordered surface with four selected representative sites for Ca, Na and K. All selected sites of cations share a close number of surface restraints around 3 with gel substrates. The gel structure of "0.8_0.3_50Na50K" serves as an example as shown. The figure on the right is the zoomed-in view of the gel structure on the xy plane.

0.2 fs.

3.3. Diffusion calculations

The variation in the composition of C-(N,K-)A-S-H alters the surface charges and textures of the gel, which influences the diffusion and transport of the ions in the nanopores as recognized by previous studies [20,21]. To gain insights into the experimental leaching outcomes of gels, we investigated the diffusion properties of cations in the nanopore of C-(N,K-)A-S-H gels with different compositions. The diffusion models

were constructed by randomly scattering sixteen NaOH or $Ca(OH)_2$ molecules in the solution of the nanopore models (Fig. 1), which aimed to mimic the mobility of cations at different distances from the gel substrates. Considering that the diffusion process was nonreactive and that the timespan was considerably long, the diffusion properties were calculated using the classical Clay force field (ClayFF) [52] with a time step of 1 fs. In ClayFF, free hydroxyl groups (OH^-) and hydroxyl of silicate (Si–OH) shared the same parameters of Lenard-Jones and quadratic bonding potentials. The detailed atomic charges in ClayFF simulations are presented in Table A1. The oxygen charge in free hydroxyl groups was -0.95 e, consistent with the original ClayFF parameters. All other atom types also retained their original ClayFF charges, except for non-bridging oxygens in the aluminosilicate chains. The charge of these oxygens was adjusted to maintain overall charge neutrality within the various C-(N,K-)A-S-H gels. We took into account the difference of Ca ions in the C-(N-)A-S-H and pore solution as how they were defined in ClayFF. The Na ions however took the same set of parameters in ClayFF.

The whole system was first equilibrated under canonical (NVT) ensemble for 1 ns with cations in the solution being fixed. Then we released the cations and ran MD simulations for 10 ns under a microcanonical (NVE) ensemble to calculate the mean square displacement as a function of time, *i.e.*, MSD(t). The diffusion coefficients of Ca and Na ions were calculated from MSD(t) based on the Einstein equation (Eq. (1)). A bin size of 7 Å was used and snapshots were recorded every 1 ps, resulting in a total of 10000 snapshots over the 10 ns simulation for the calculation of MSD and diffusion coefficients. While the pore solution of C-(N,K-)A-S-H gels was well-known to be alkaline, containing Na, K, and Ca ions [23], accurately determining the exact ion concentration remains challenging. In practice, the solubility of cations within a 5 nm pore solution box was constrained. Therefore, to ensure sufficient ion statistics for analysis while minimizing the number of introduced ions, 16 Na (or Ca or K) ions were selected for diffusion coefficient calculations.

$$D = \frac{1}{2N}\lim_{t\to\infty}\frac{MSD(t)}{t} \quad (1)$$

where N = 3 is the dimensionality for the bulk diffusion.

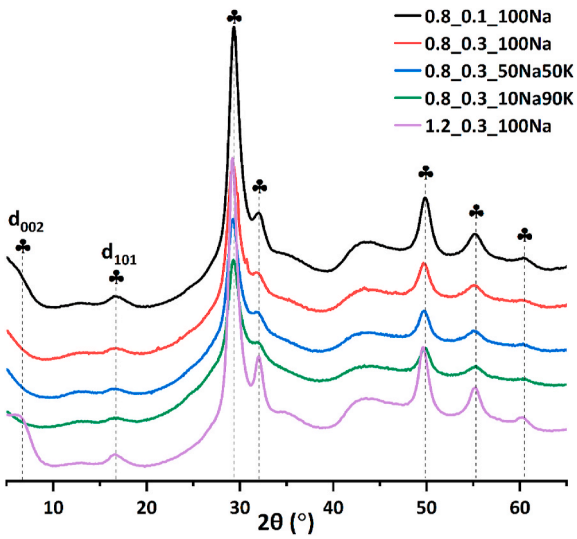

Fig. 4. XRD pattern of the synthetic gels. ♣: C-(N,K-)A-S-H gels.

4. Results

4.1. Phase assemblage

As observed in Fig. 4, representative reflections corresponding to 14 Å tobermorite [PDF# 00-029-0331] are identified in the synthetic gels, which indicates the presence of the high-purity C-(N,K-)A-S-H gel. The intensity of these characteristic peaks changes with the variation of Ca/Si and Al/Si ratios. For instance, the peak referring to d_{002}, located between 5 and 10°, correlates with the property of basal spacing. It is reported in [32] that the signal in the gel with a higher Ca/Si ratio is more pronounced than that with a low Ca/Si ratio. This is in agreement with our results, in which an evident reflection regarding d_{002} is discernible exclusively in the gel with a Ca/Si ratio of 1.2. This phenomenon likely arises for two main reasons. First, the gel with a lower Ca and a higher Al content possesses a larger interlayer distance [31], potentially resulting in a lower peak value of d_{002} below 5°. Second, the gel with a lower Ca and higher Al content tends to exhibit a less ordered and more cross-linked structure [8], leading to a faint reflection of the characteristic 14 Å tobermorite. This hypothesis is supported by the observation that the intensity of characteristic peaks is generally higher in the 1.2_0.3_100Na gel than in the other four gels. Additionally, the presence of d_{101} peak is also detected across all five gels, which is considered as the Si in bridging sites in gels [53]. Notably, the inclusion of potassium in the gels does not significantly alter the gel structure, as demonstrated by the comparison among the three 0.8_0.3 gels.

4.2. Leaching behaviour of synthetic gels

The leaching behaviours of the five gels were systematically monitored, including the structure formers (Si and Al) and structure modifiers (Ca, Na, and K). The leaching amount and the leaching ratio of different ions were measured and calculated in this section. The leaching amount of a certain ion is prominently dependent on its inherent content in gels [11], whereas the leaching ratio can mirror the leaching stability of ions. We initially examined the 0.8_0.1_100Na, 0.8_0.3_100Na, and 1.2_0.3_100Na gels to investigate the influence of Ca/Si and Al/Si ratios on the leaching of ions. Then, the gels of 0.8_0.3_100Na, 0.8_0.3_50Na50K, and 0.8_0.3_10Na90K were compared to understand the discrepancy of leaching behaviour among Ca, Na and K in a gel with similar Ca/Si and Al/Si ratios.

4.2.1. C-(N-)A-S-H gels

Fig. 5 shows the leaching behaviours of Si and Al in the three C-(N-)A-S-H gels with time. Generally, ion concentrations increase with leaching time, with most ions reaching a steady state after 360 min of water immersion. This rapid leaching behaviour of the synthetic gels contrasts with that in pastes or concrete, where the dense matrix slows ion leaching. As shown in Fig. 5A and B, the profiles for both ion concentration and the leaching ratio of Si are similar. Notably, the gel with a lower Ca/Si ratio shows a higher leaching ratio of Si, which suggests that the presence of Ca enhances the stability of Si within gels. Additionally, the leaching ratio of Si in the 0.8_0.3_100Na gel is slightly higher than in the 0.8_0.1_100Na gel. This is probably attributed to the marginally lower Ca/(Si + Al) ratio of the 0.8_0.3_100Na gel (0.74) than that of the 0.8_0.1_100Na gel (0.77) (Table 2).

Fig. 5C shows the ion concentration of Al in the leachate of gels with time. The 0.8_0.3_100Na gel exhibits the highest Al concentration, followed by the gels of 1.2_0.3_100Na and 0.8_0.1_100Na. Given that the initial content of Al in the 0.8_0.3_100Na gel is higher than in the other two, it naturally results in a higher leaching amount. Fig. 5D shows the leaching ratio of Al in gels with time. Comparing the 0.8_0.1_100Na and 0.8_0.3_100Na gels, it is evident that an increased content of Al leads to a higher leaching ratio of Al. This implies that the extra Al in the 0.8_0.3_100Na gel shows high leaching potential, probably due to the presence of $[AlO_5]$ and $[AlO_6]$ in the interlayer [17]. Additionally,

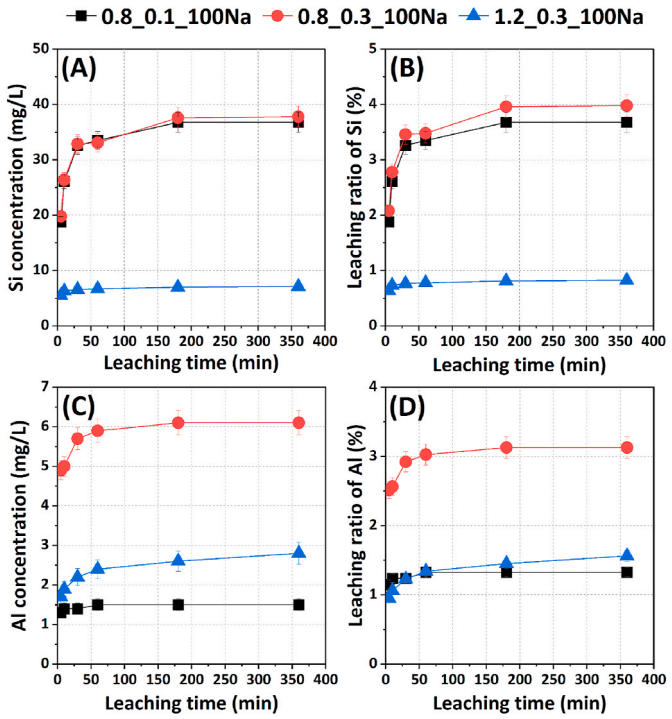

Fig. 5. Leaching behaviours of Si and Al in C-(N-)A-S-H gels within 360 min. **(A)** and **(C)**: Si and Al concentrations in the leachate of gels with time. **(B)** and **(D)**: leaching ratios of Si and Al in gels with time.

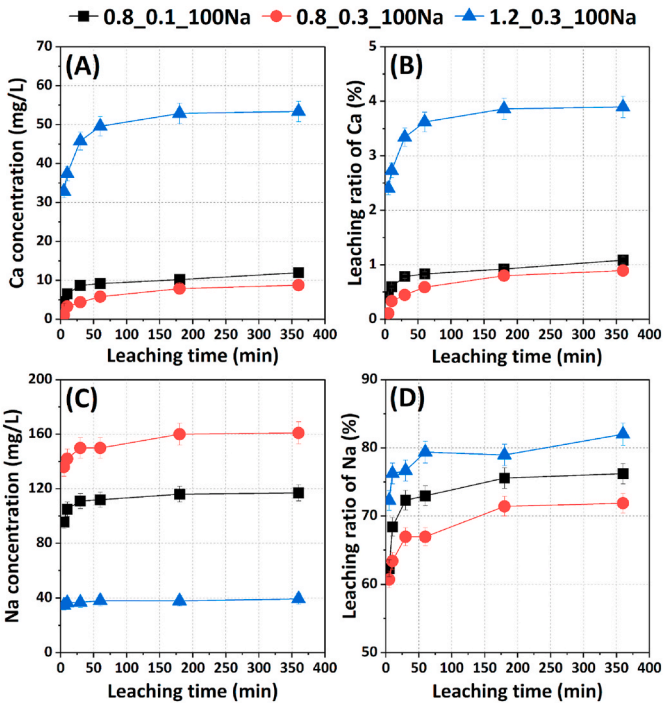

Fig. 6. Leaching behaviour of Ca and Na in C-(N-)A-S-H gels within 360 min. **(A)** and **(C)**: Ca and Na concentrations in the leachate of gels with time. **(B)** and **(D)**: leaching ratios of Ca and Na in gels with time.

comparing the 0.8_0.3_100Na and 1.2_0.3_100Na gels, the one with a higher Ca/Si ratio shows a lower leaching ratio of Al. This suggests that the presence of Ca enhances the immobility of Al, consistent with the results of Si (Fig. 5B). These findings agree well with the gel solubility results reported in [11] and confirm that Ca is essential to the leaching stability of both Si and Al tetrahedral in gels.

Fig. 6A and B shows the leaching behaviour of Ca in C-(N-)A-S-H gels with time. Both the ion concentration and leaching ratio of Ca follow a coherent trend across the three gels. The gel with a higher Ca/(Si + Al) ratio shows a higher leaching amount and ratio of Ca, primarily due to the initial distribution of Ca in gels. Typically, Ca exists in two forms within the gel structure: intralayer Ca and interlayer Ca [37]. Intralayer Ca is embedded within the CaO sheet and is generally resistant to dissolution unless the structure undergoes severe failure. In contrast, the interlayer Ca serving as the charge-balancing ion in between the CaO sheets is relatively more mobile and is the main source of leached Ca ions [22]. Due to the low content of Ca in the 0.8_0.1_100Na and 0.8_0.3_100Na gels, the responsibility of compensating the charge is extensively taken over by Na ions. This results in a deficiency of Ca ions in the interlayer and consequently a lower leaching amount of Ca.

Fig. 6C shows the ion concentration of Na in the leachate of gels with time. Overall, the concentration of Na is notably higher than that of Si, Al, and Ca, indicating a relatively weak interaction between Na and gels. Additionally, the gel of 0.8_0.3_100Na shows the highest leaching amount of Na, followed by the 0.8_0.1_100Na and 1.2_0.3_100Na gels. This is primarily due to a higher initial Na content in the 0.8_0.3_100Na gel (Table 2). Interestingly, the trend of the leaching ratio of Na is contrary to that of the leaching amount. As observed in Fig. 6D, the gel of 1.2_0.3_100Na shows the highest leaching ratio of Na, while the gel of 0.8_0.3_100Na shows the lowest. This implies that the gel with an increased Ca/Si ratio and a decreased Al/Si ratio has a higher leaching potential of Na. The gel with a higher Ca or a lower Al content shows a more positively charged surface, which in turn promotes the dissolution of Na ions (each carrying a single positive charge). This statement will be further corroborated by MD simulation results.

4.2.2. C-(N,K-)A-S-H gels

Fig. 7 shows the ion concentration of Si and Al in the leachate, as well as the leaching ratio of Si and Al in C-(N,K-)A-S-H gels. The gel of 0.8_0.3_100Na exhibits the highest leaching amount and ratio for both Si and Al compared to the gels of 0.8_0.3_50Na50K and 0.8_0.3_10Na90K. Interestingly, as presented in Table 2, the gels of 0.8_0.3_50Na50K and

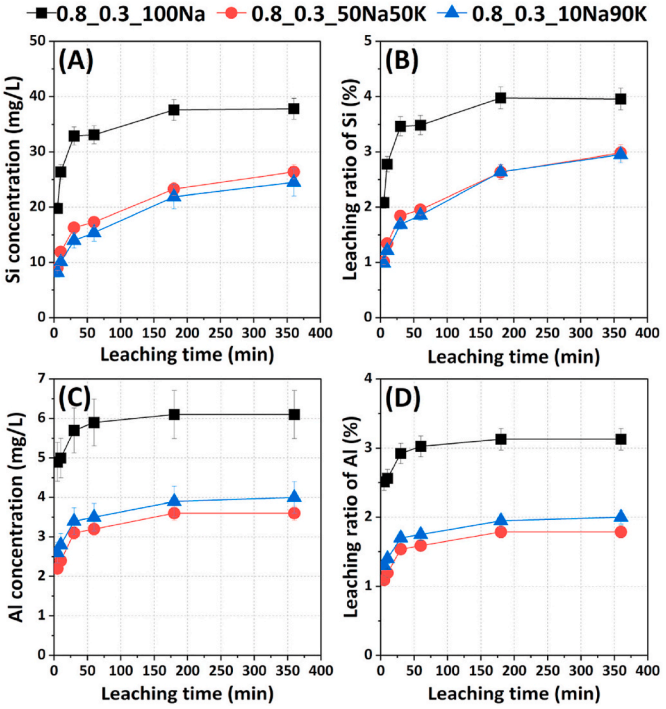

Fig. 7. Leaching behaviour of Si and Al in C-(N,K-)A-S-H gels within 360 min. **(A)** and **(C)**: Si and Al concentrations in the leachate of gels with time. **(B)** and **(D)**: leaching ratios of Si and Al in gels with time.

0.8_0.3_10Na90K show higher contents of Si and Al than the gel of 0.8_0.3_100Na. These findings suggest that the presence of K contributes to the immobility of Si and Al. A possible explanation is that K has a higher effective charge than Na, which facilitates its ability to bind with Si or Al tetrahedral, thereby stabilizing these components in the gel matrix. Further discussion is available in section 5.2.

Fig. 8 shows the leaching behaviour of Ca, Na and K in C-(N,K-)A-S-H gels with time. As shown in Fig. 8A and B, the 0.8_0.3_100Na gel shows the highest leaching amount and ratio of Ca, followed by the gels of 0.8_0.3_50Na50K and 0.8_0.3_10Na90K. This indicates that the presence of K reduces the leaching of Ca, possibly because the gels with a higher K content have a correspondingly lower Ca content as indicated in Table 2. Fig. 8C shows the ion concentration of Na in the leachate of the three gels. The gel with a higher initial Na content shows a higher equilibrium concentration. However, as shown in Fig. 8D, the leaching ratio of Na in the 0.8_0.3_10Na90K gel is higher than in the other two gels. This indicates that the presence of K promotes the leaching of Na. In C-(N,K-)A-S-H gels, both Na and K ions serve as charge-balancing ions in the interlayer, implying potential competition between them. Hence, a preferential dissolution of Na ions over K ions under the same conditions could also be contributing to the observed trend.

Fig. 8E and F show the leaching behaviour of K in gels with time. While the leaching amount and ratio of K are lower than that of Na, they remain substantially higher compared to Si, Al and Ca. As shown in Fig. 8B–, D and F, the leaching ratio of Na (70–80 %) is higher than that of K (45–55 %), and both are much higher than that of Ca (0.4–1.0 %). This indicates that the leaching resistance of Ca is significantly stronger than Na and K, while K exhibits a higher resistance than Na. Despite both Na and K belonging to the same elemental group, their leaching behaviours are different, probably attributed to their different ionic radius and dissolution free energies. Further discussion is provided in section 4.4.

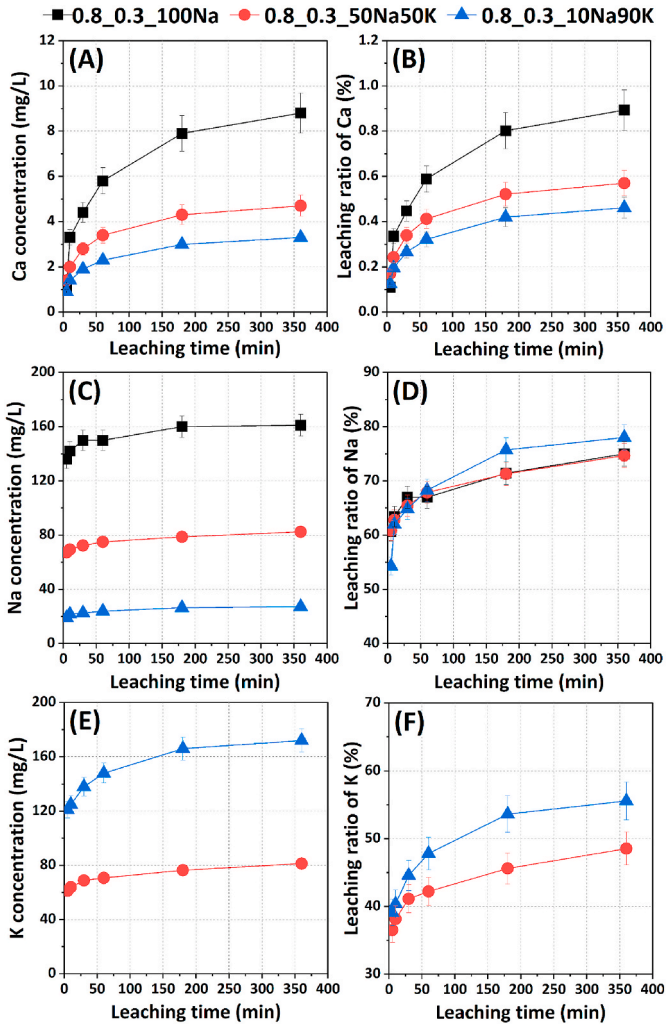

Fig. 8. Leaching behaviour of Ca, Na and K in C-(N,K-)A-S-H gels within 360 min. **(A)(C)(E)**: Ca, Na and K concentrations in the leachate of gels with time. **(B)(D)(F)**: leaching ratios of Ca, Na and K in gels with time.

4.3. Chemical environments of Na

The central transition of ^{23}Na NMR spectra for the five synthetic C-(N,K-)A-S-H gels before leaching is shown in Fig. 9A, demonstrating a featureless sharp resonance near -2 ppm, without clear second-order quadrupolar broadening. This resonance can be assigned to the outer-sphere hydrated Na ions ($[Na(H_2O)_x]^+$, $0 \leq x \leq 6$) located on the surface of gels or intercalated within the interlayer structure [54,55]. The intensities of the ^{23}Na NMR spectra have been corrected for the actual sample amounts, packed in the rotor for the ^{23}Na NMR experiments. These intensities can be used for the quantification of the amount of Na ions present in gels. For the three C-(N-)A-S-H gels, the 0.8_0.3_100Na gel shows the highest intensity of Na, followed by the 0.8_0.1_100Na gel, while the 1.2_0.3_100Na gel shows the lowest Na content. These results are consistent with the chemical composition determined by XRF (Table 2), which indicates that the Na amount in the gels increases with a decreasing Ca/Si ratio and an increasing Al/Si ratio. When Na is partially substituted by K, a clear decrease in the Na content of C-(N,K-)A-S-H gels is observed, as evidenced by the lower intensities of ^{23}Na NMR spectra. This suggests that K takes a similar role as Na in gels, *i.e.* charge compensator.

A small shift of the centre of gravity (δ_{cg}) of the ^{23}Na NMR spectra towards higher frequency is observed for the C-(N,K-)A-S-H gels, whereas the C-(N-)A-S-H gels show comparable values (Fig. 9B). This shift may indicate an increase of coordination number of Na ions with water molecules, *e.g.* obtained by weaker bonding of Na to the C-(N,K-)A-S-H gels, due to the substitution of Na by K. Moreover, the linewidths of ^{23}Na NMR spectra, obtained from the full width at half maximum (FWHM), of K-containing gels are slightly narrower than the K-free gels (Fig. 9C). The reduction of spectral linewidth may ascribe to the higher mobility or stronger dynamic processes for Na ions, caused by weaker bonding associated the gels with the substitution of Na by K. This is further supported by the leaching data in Fig. 8D, where the gel with higher K substitution level (0.8_0.3_10Na90K) shows higher Na leaching ratio than the other two gels with similar Ca/Si and Al/Si ratios (0.8_0.3_100Na and 0.8_0.3_50Na50K). The δ_{cg} of ^{23}Na NMR spectra shifts to higher frequency due to the substitution of Na by K was also reported by Duxon et al. [56]. The δ_{cg} of ^{23}Na NMR spectrum for the geopolymer prepared by a hybrid activator (Na:K = 1:1) shifts to a higher frequency as compared to that of the sample prepared with pure Na-based activators.

4.4. Dissolution free energy of Ca, Na and K ions

In this section, we first compare the dissolution free energies of Ca and Na in three C-(N-)A-S-H gels to investigate the impact of chemical composition on the leaching potential of cations. Then, we calculated the dissolution free energy of Ca, K, and Na in an identical gel (0.8_0.3_50Na50K) to understand their leaching potential in gels.

Fig. 10 illustrates a 2D map depicting the dissolution free energies of Ca and Na from C-(N-)A-S-H gels as a function of both the dissolution distance and the coordination number of cations with gels. Here, "cation-Os" denotes the coordination number of surface cations with the oxygen atoms in the silicate/aluminate chains, which accounts for the number of restraints on the surface cations [22]. Only the dissolution distance along the z-axis is considered, since their movement along the x- and y-axes is confined by other ions on the gel surface. Each system

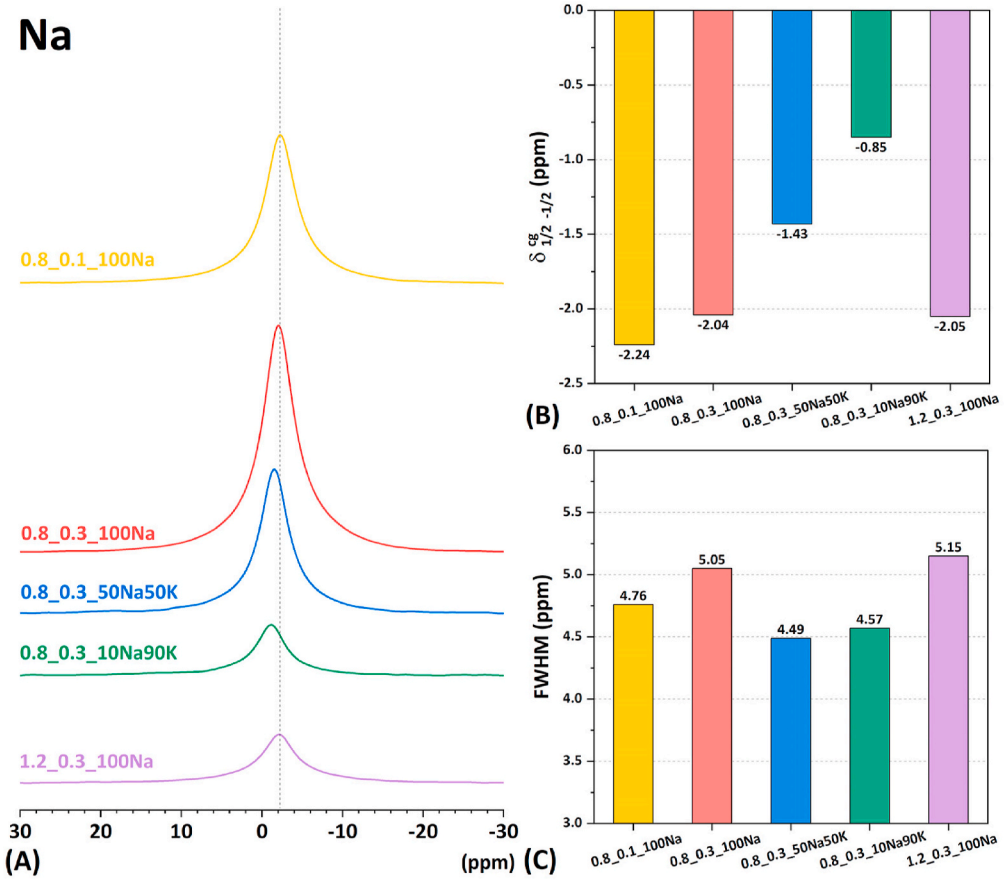

Fig. 9. (A) ^{23}Na NMR spectra (14.1 T, $\nu_R = 25.0$ kHz) of five C-(N,K-)A-S-H gels with different chemical compositions before being exposed to water. **(B)** the centre of gravity for the central transition ($\delta^{cg}_{1/2,-1/2}$) of the spectra. **(C)** Full width at half maximum (FWHM) of the spectra.

undergoes multiple free energy minima (intermediate states) and saddle points (transition states) until the cations are fully dissolved. The difference in free energy between the minimum points and saddle points represents the dissolution free energy barrier, which is inversely related to the ease of cation dissolution. In general, the free energy barrier increases with the coordination number, as the dissolution of cations becomes more difficult with the increase of restraints. Additionally, the initial dissolution position on the x-axis is below zero, as an indicator of the initial absorption of cations by gels. This is probably due to the presence of vacancies and defects on the surface of C-(N-)A-S-H gels [22].

Fig. 10A–C show the dissolution free energy of Ca ions from three C-(N-)A-S-H gels. Initially, Ca shows a coordination number of 2–5 with the surface oxygen atoms of gels. As dissolution progresses, Ca gradually detaches from the surface, resulting in a decrease in cation-Os (*i.e.* more surface restraints are broken) until it reaches zero. The general profile of the free energy landscape of Ca is similar across the three gels, whereas the gel of 0.8_0.3_100Na shows a larger energy barrier, as indicated by the red regions (deep free energy basin) in Fig. 10B.

Fig. 10D–F show the dissolution free energy of Na from three C-(N-)A-S-H gels. The initial coordination number of surface Na ions is comparable to Ca before dissolution. However, the gradient of free energy of Na is much shallower, indicating a lower energy barrier for dissolution and thus a higher leaching potential. Interestingly, the initial coordination number of surface Na in the gel of 1.2_0.3_100Na (Fig. 10F) is lower than in the other two gels. This reduction in coordination with the gel matrix is probably due to the higher Ca/Si ratio of gels. The gel with a higher Ca/Si ratio shows a shorter mean chain length [14], which makes it more accessible to water molecules. Consequently, the Na ions at the gel surface experience enhanced interaction with water and reduced interaction with the gel.

Based on the free energy landscape, the overall dissolution free energy barrier can be calculated by searching the transition states using the nudged elastic band method [57]. Considering the complexity of gel surfaces, we calculated the average dissolution free energies of four representative sites for each type of cation (Fig. 3). The average dissolution free energy for Ca and Na are compared in Fig. 11. It can be seen that the dissolution free energy of Ca is generally higher than that of Na, consistent with the leaching result (Fig. 6). Additionally, both Ca and Na in the gel of 0.8_0.3_100Na have higher dissolution free energy than in the other two gels, which indicates that cations in the gel with a lower Ca/Si ratio and a higher Al/Si ratio show lower leaching potential. In addition, the dissolution free energy of the 1.2_0.3_100Na gel is lower than the 0.8_0.1_100Na gel, which suggests that the effect of an elevated Ca/Si ratio in promoting the dissolution of cations is larger than that of a reduced Al/Si ratio. These findings align well with the experimental results shown in Fig. 7, likely due to the difference in the surface charge of gels.

Fig. 12 shows the 2D dissolution free energy landscape of Ca, K and Na from the gel of 0.8_0.3_50Na50K as a function of coordination number with gels and dissolution distance. Among the three cations, Ca ions exhibit the most complex dissolution steps and the highest free energy barrier, followed by K and then Na, indicating that the dissolution of Ca is much more difficult than the other two ions. Fig. 13 shows the average dissolution free energy for Ca, K, and Na, indicating that the leaching potential of cations from identical C-(N,K-)A-S-H gels follows the order: Ca < K < Na. This aligns with the leaching results shown in Fig. 8. Furthermore, the dissolution free energy of Na in the gel of 0.8_0.3_50Na50K (~30 kJ/mol) is slightly lower than in the gel of 0.8_0.3_100Na (~32 kJ/mol). This suggests that the incorporation of K

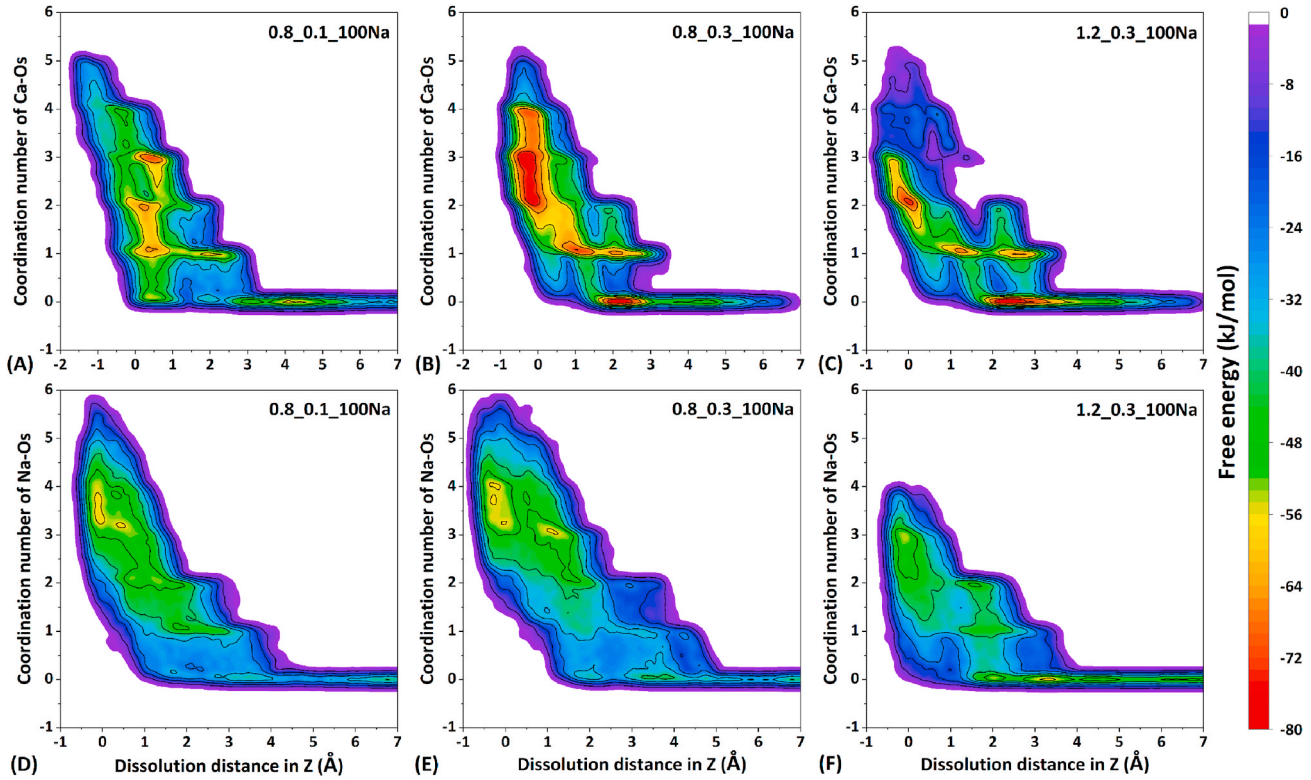

Fig. 10. 2D dissolution free energy landscape for Ca and Na from the gels of "0.8_0.1_100Na", "0.8_0.3_100Na" and "1.2_0.3_100Na" as a function of dissolution distance and "cation-Os" coordination number (*i.e.*, number of surface restraints). "Os" refers to the surface oxygen of the solid (gels). The maximum free energy in each system is normalized by zero.

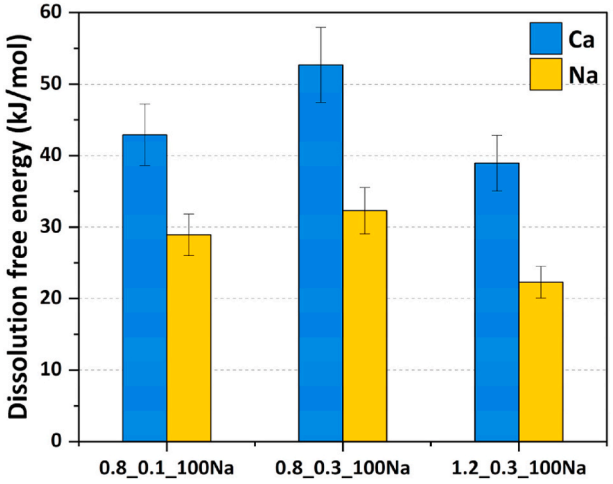

Fig. 11. The average dissolution free energy barrier (between the transition state and initial state) of Ca and Na located at four representative sites. The average dissolution free energy of Ca in the three gels is ~43, ~53 and ~39 kJ/mol, respectively. The average dissolution free energy of Na in the three gels is ~29, ~32 and ~22 kJ/mol, respectively.

promotes the dissolution of Na, which agrees with both the leaching result (Fig. 8) and the ^{23}Na NMR result (Fig. 9).

4.5. Diffusion coefficient of Ca and Na in the nanopore of gels

In this section, we investigate the diffusion behaviour of Ca and Na ions at different distances from the gel substrate. Atomic density distribution refers to the spatial distribution of atoms within the system. It involves analyzing the quantity or concentration of atoms in different regions of the simulated space. Fig. A1 shows the atomic density distributions of Ca and Na ions along the Z direction (Z = 42–92 Å) in the nanopore with time. At the very beginning (t = 0), Ca and Na ions are uniformly distributed in the nanopores. As the simulation proceeds, however, the atomic density of both cations becomes higher near the gel substrates, which indicates that the cations are to some extent adsorbed onto the upper and lower surfaces of C-(N-)A-S-H gels. This is due to the negative surface charges of gels, as documented in previous work [58,59]. This adsorption capacity reflects the ability of C-(N-)A-S-H gels in bearing cations and serves as an indicator to inversely compare the ease of cation leaching from the gel.

To quantitively describe the mobility of cations impacted by the absorption of gel surfaces in confined nanopore water, the diffusion coefficients of Ca and Na ions were calculated using the trajectory of cations at various distances from the gel substrates, as shown in Fig. 14. In general, the diffusion coefficient of Na ions is higher than that of Ca ions at equivalent locations within the nanopore. This is mainly due to a higher intrinsic diffusion coefficient of Na than Ca [60,61]. Additionally, the diffusion coefficient of both cations in proximity to the gel substrate is notably lower than that of ions positioned in the middle of the nanopore. This further confirms the adhesive behaviour of the gel substrates.

Fig. 15 illustrates the average diffusion coefficients of Ca and Na ions in the nanopore between the C-(N-)A-S-H gel substrates. The average diffusion coefficient of Ca ions is consistently lower than that of Na ions in all three gels. Additionally, the diffusion coefficient of both Ca and Na ions in the gel of 1.2_0.3_100Na is higher than that in the gels of 0.8_0.1_100Na and 0.8_0.3_100Na. This indicates that a high Ca/Si ratio results in less effective absorption of cations. On the other hand, the comparison of the diffusion coefficient of Na between the 0.8_0.1_100Na and 0.8_0.3_100Na gels implies that a higher Al incorporation promotes the absorption of Na. The average diffusion coefficient of K in the

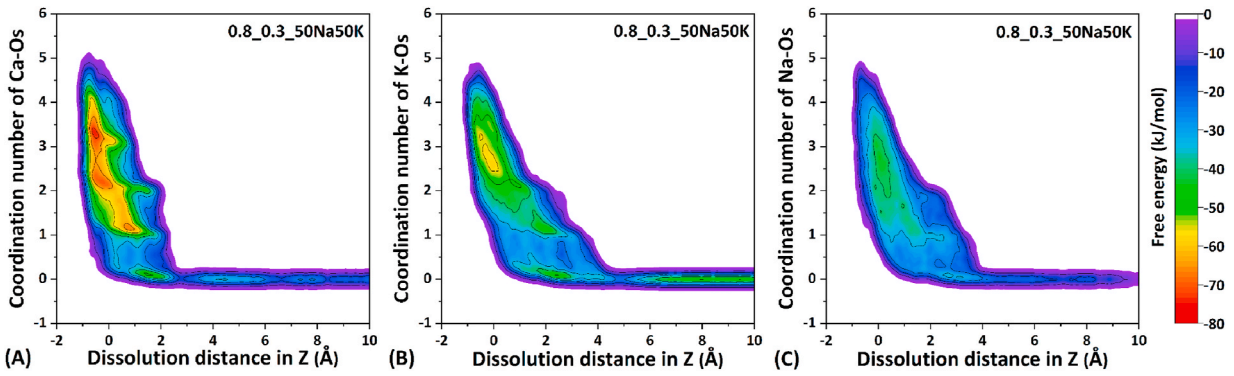

Fig. 12. 2D dissolution free energy landscape for Ca, K and Na from the gel of 0.8_0.3_50Na50K as a function of dissolution distance and cation-Os coordination number (*i.e.*, number of surface restraints). "Os" refers to the surface oxygen of the solid (gels). The maximum free energy in each system is normalized by zero.

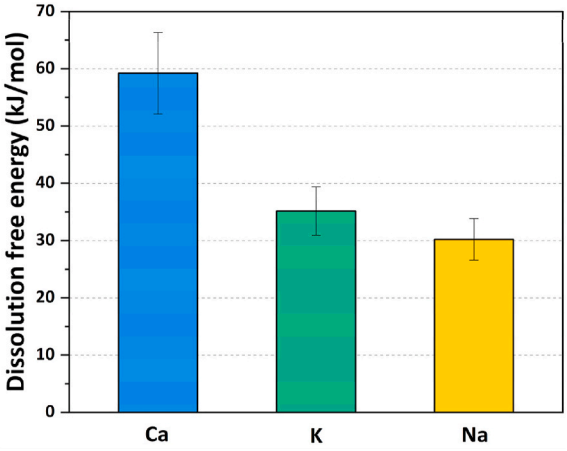

Fig. 13. The average dissolution free energy barrier (between the transition state and initial state) of Ca, K, and Na located at four representative surface sites of the 0.8_0.3_50Na50K gel. The average dissolution free energies of Ca, K, and Na are ~59, ~35, and ~30 kJ/mol, respectively.

nanopore of the two C-(N,K-)A-S-H gels was also calculated, as shown in Fig. A2. It is observed that the mobility of K is higher than that of Ca and Na. As the cations are free in the nanopore solution, their diffusion coefficients are more dependent on their intrinsic properties. Under aqueous conditions, K has a larger ionic radius than Na, and the hydration shell formed by water molecules around K is more loosely bound than that around Na. As a result, the friction between hydrated K ions and surrounding water molecules is lower than that of Na, resulting in higher mobility of K [61].

5. Discussion

5.1. Impact of gel chemistry on the dissolution potential of cations

Fig. 16 shows the relationship between the dissolution free energy and diffusion coefficient of Ca and Na in the three C-(N-)A-S-H gels. It is observed that the dissolution free energy of both Ca and Na is negatively correlated with their respective diffusion coefficients. As for the same cation, the diffusion coefficient is closely related to the charge on the gel surface. Therefore, this indicates that the binding energy between gels and cations is also related to the surface properties of gels. More specifically, the gel with a lower Ca/Si ratio and a higher Al/Si ratio shows increased surface negativity, which strengthens the binding between cations and gel substrates, thereby hindering the dissolution potential of cations.

5.2. Mechanisms behind the different dissolution potential of cations

Typically, the discrepancy in the dissolution of cations is dependent on the interaction between cations and silicic (or aluminium) acid anions, a concept explained by the electric double-layer theory and the charge screening effect of cations [62–64]. Fig. 17A shows the schematical representation of the electric double layer surrounding a silicic acid anion and Fig. 17B shows the potential energy distributed in these layers. When these anions (*e.g.,* $SiO(OH)_3^-$ or $SiO_2(OH)_2^{2-}$) are present in an electrolytic solution, a double layer forms around their charged surface. Positively charged species from the solution are attracted to this surface, resulting in a higher concentration of ions in the absorbed layer (double layer) compared to the adjoining bulk solution. The inner part of this absorbed layer is known as the "Helmholtz layer" or "Stern layer" [65], which is tightly bound to the surface. The outer part of this absorbed layer is designated as the "diffusion layer", where the force from the anion gradually diminishes, eventually reaching an equilibrium with that of the bulk solution, as the distance from the Stern layer increases.

The formation of silicate chains involves the condensation of Si or Al tetrahedrons, and the strength of binding between two anions is closely associated with the property of a double layer. As the two anions approach each other in a solution, there exists a certain distance at which they begin to experience a repulsive force. This force, represented by the total potential energy, is determined by the competition between repulsive potential energy and attractive potential energy (Van der Waals), as shown in Fig. 17C. It can be seen that the gel condensation process can only occur if the two anions collide with sufficient velocity to overcome this potential barrier. However, this barrier can be substantially lowered through the addition of cations, which can form a shielding double layer. This shielding effect of cations is particularly effective at a higher valence [67,68], as shown in Fig. 17D. The previous results have shown that the required ion concentration of monovalent alkali metal ions (Li, Na, K) for gel condensation is nearly 100 times higher than that of divalent alkali earth metal ions (Mg, Ca, Ba) [68]. This indicates that Ca is more effective than Na and K in promoting gel formation, thereby the binding between Ca ions and Si/Al anions is more robust. As a result, the leaching potential of Ca ions is lower than that of Na and K ions.

However, the aforementioned theory may not fully explain the difference in dissolution free energy between Na and K ions, as both of them belong to monovalent alkali metal ions. The charge screening effect of cations needs to be taken into account. Fig. 17E and F show the schematical illustration of the surrounding environments of Na and K ions in a hydrated condition. Due to the polarity of water molecules, the hydrolysis of cations happens in an aqueous solution, resulting in a slightly positive charge at H atoms and a slightly negative charge at O atoms. The layer of water molecules surrounding cations forms a tightly bound hydration shell, regarded as a solid part of hydrated cations. It is

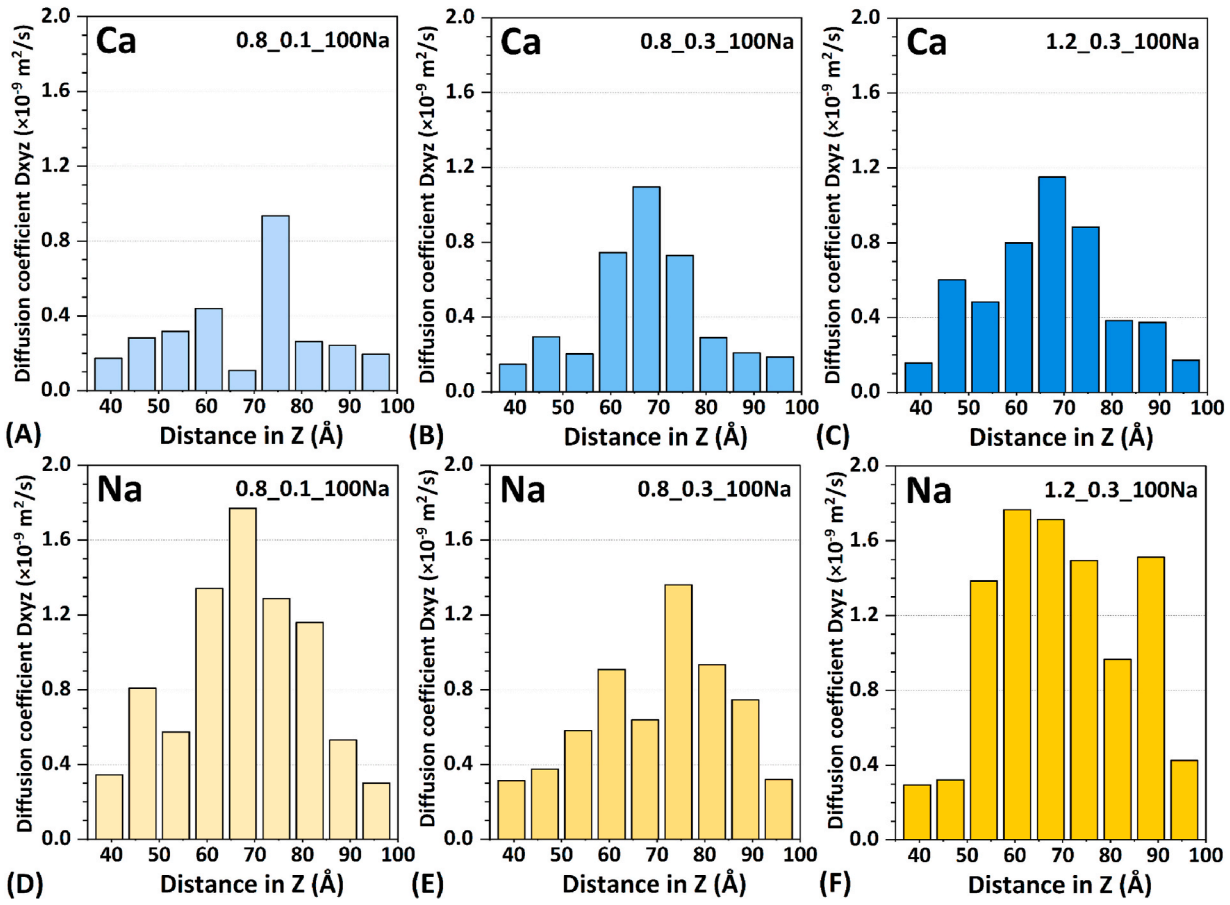

Fig. 14. Diffusion coefficient distributions of Ca and Na ions along the Z-axis of the nanopore solution perpendicular to the surface of the gels of "0.8_0.1_100Na", "0.8_0.3_100Na" and "1.2_0.3_100Na". In each inset, the locations near 40 Å and 95 Å at the "distance in Z" correspond to the gel substrates while that at 67 Å is near the centre of the nanopore of gels.

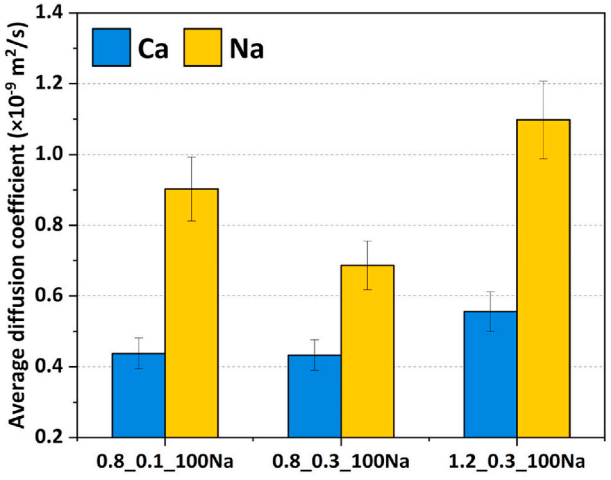

Fig. 15. Average diffusion coefficients of Ca and Na ions in the nanopore of the gels of "0.8_0.1_100Na", "0.8_0.3_100Na" and "1.2_0.3_100Na". The average diffusion coefficients of Ca ions in the three gels are 0.44, 0.43 and 0.56 × 10^{-9} m^2/s, respectively. The average diffusion coefficients of Na ions in the three gels are 0.9, 0.69 and 1.1 × 10^{-9} m^2/s, respectively. The error bars represent the standard deviation calculated from 16 individual measurements.

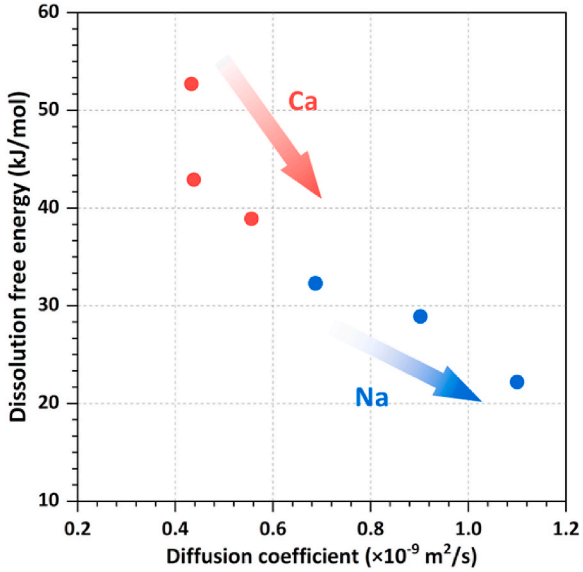

Fig. 16. Relationship between the dissolution free energy and diffusion coefficient of Ca and Na in the gels of "0.8_0.1_100Na", "0.8_0.3_100Na" and "1.2_0.3_100Na".

reported that the cations with the same valence but smaller radius exhibit stronger bonding with hydrated water molecules [67]. This statement is consistent with our simulation results (Fig. A3) regarding the radial distribution function (RDF) of Na-O_W and K-O_W (O_W indicates the oxygen in water molecules). As shown in Fig. A3, the bond length of Na-O_W (~2.35 Å) is significantly shorter than that of K-O_W (~2.85 Å),

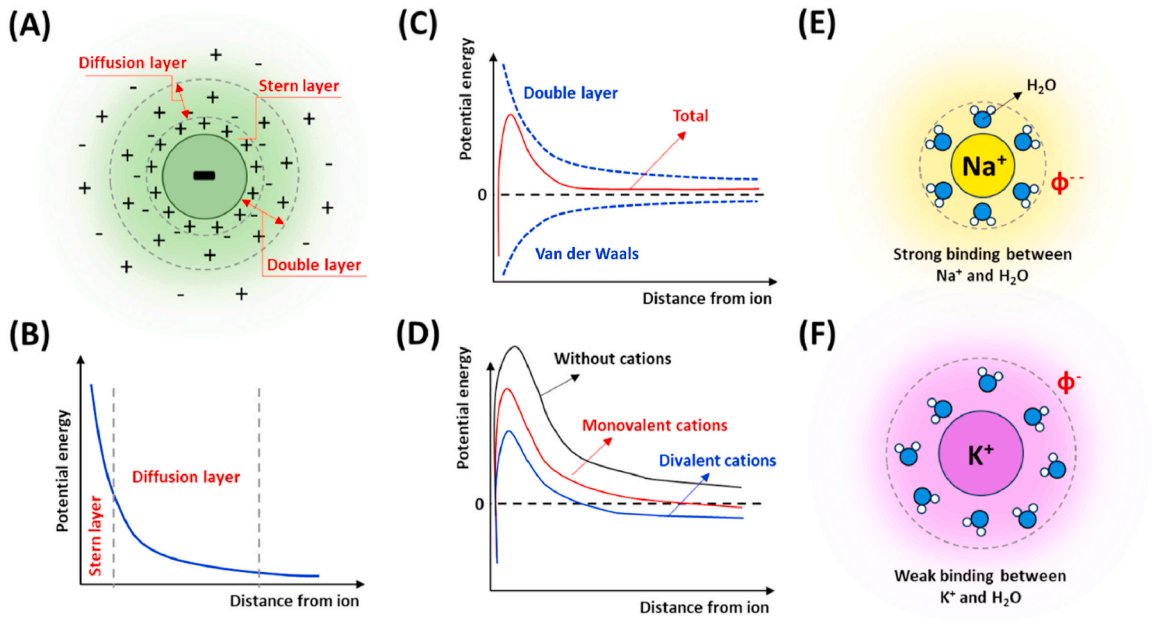

Fig. 17. Schematic representation of **(A)** electric double layer distribution surrounding an anion [66]; **(B)** potential energy distribution surrounding a sole anion [66]; **(C)** potential energy distribution between two approaching anions [64]; **(D)** potential energy distribution in the presence of cations with different valences [64]; **(E)** local chemical environment of a hydraulic Na ion; **(F)** local chemical environment of a hydraulic K ion. ϕ^{--} and ϕ^{-} indicate that the charge shielding by water molecules around Na ions is larger than K ions.

indicating a stronger binding and charge screening effect of Na-O_W. As a consequence, K ions retain a higher positive charge and are more effective in balancing the charge within the gel interlayer. The binding between K ions and the gel surface is stronger than that of Na ions. This result not only explains the lower dissolution potential of K than Na but also elucidates why materials activated by K-based activators show higher compressive strength than those activated by Na-based ones [69, 70].

5.3. *Perspective on the dissolution of cations in gels*

During the MD simulation process, we observed that some OH^- ions can leach away from gel substrates along with cations. This might indicate the increase in the pH of the host solution. However, the variation of pH due to the dissolution of cations is not considered in this study, since our focus is primarily on the dissolution behaviour of limited cations at very early ages, which may not significantly impact the pH of the host solution on their own. In reality, the leaching of gels results in elevated pH in the solution [14]. The increase in pH can influence the solubility of various species, including cations, and can alter the kinetics and thermodynamics of dissolution processes. Understanding these complex interactions between pH changes, cation dissolution, and the stability of gels is crucial for accurately modelling and predicting the behaviour of these materials in practical applications. The insights of this work contribute to tailoring the chemical composition of gels to minimize leaching and further optimizing the mixture design of AAMs. Further investigations into these reactions are warranted to comprehensively grasp their implications and optimize the performance of gels in various environmental and engineering contexts.

6. Conclusions

In this work, the dissolution behaviour of cations (Ca, Na and K) from C-(N,K-)A-S-H gels was investigated by experiments. The underlying mechanisms were revealed by MD simulation. Several conclusions can be drawn as follows.

1. The gel with a higher Ca content showed an increased degree of crystallization. The influence of Na and K on the gel structure was comparable. In addition, an increased content of Ca and K enhanced the immobilization of Si and Al.
2. An elevated Ca/Si ratio and a reduced Al/Si ratio of gels promoted the dissolution of cations. This was because a higher Ca/Si ratio and a lower Al/Si ratio reduced the charge negativity of gel surfaces, resulting in weaker binding and absorption between cations and gel surfaces. Additionally, the gel with a higher Ca/Si ratio featured a shorter and more defective aluminosilicate chain, which resulted in fewer surface restraints on cations, lessening the prohibition of ion leaching.
3. The gel with the incorporation of K showed a higher leaching potential of Na. The ^{23}Na NMR spectra showed that the presence of K weakened the binding between Na and gels and enhanced the mobility of Na within the gels. The MD simulation results also indicated that the dissolution free energy of Na in K-containing gels was slightly lower than in K-free gels.
4. In the gel of 0.8_0.3_50Na50K, the dissolution free energies of Ca, K and Na were ~59 kJ/mol, ~35 kJ/mol and ~30 kJ/mol, respectively. This accounted for the higher dissolution potential of Na and K than Ca. This was attributed to the binding between cations and the gel, which was influenced by both the valence and the effective charge of the cations.

CRediT authorship contribution statement

Chen Liu: Writing – original draft, Methodology, Investigation, Conceptualization. **Yong Tao:** Writing – review & editing, Methodology, Conceptualization. **Shuai Nie:** Methodology. **Yun Chen:** Investigation. **Zhenming Li:** Writing – review & editing, Supervision. **Chi Sun Poon:** Writing – review & editing. **Guang Ye:** Writing – review & editing, Supervision.

Declaration of competing interest

The authors declare that they have no known competing financial interests or personal relationships that could have appeared to influence

the work reported in this paper.

Acknowledgement

Chen Liu and Yun Chen would like to acknowledge the funding supported by the China Scholarship Council (CSC) under grants No. 201906950102 and No. 201906150022, respectively. Zhenming Li would like to acknowledge the Guangdong Provincial Key Laboratory of Intelligent and Resilient Structures for Civil Engineering (2023B1212010004).

Appendix

Fig. A1 shows the atomic density profiles of Ca and Na ions along the Z-axis of 5 nm nanopore of three C-(N-)A-S-H gels with simulation time. The 1.2_0.3_100Na gel shows a higher atomic density of Na than the gels of 0.8_0.1_100Na and 0.8_0.3_100Na in the middle of the nanopore at the simulation time τ. This means that the effect of electrostatic adhesion is less intensive in the gel with a higher Ca/Si ratio.

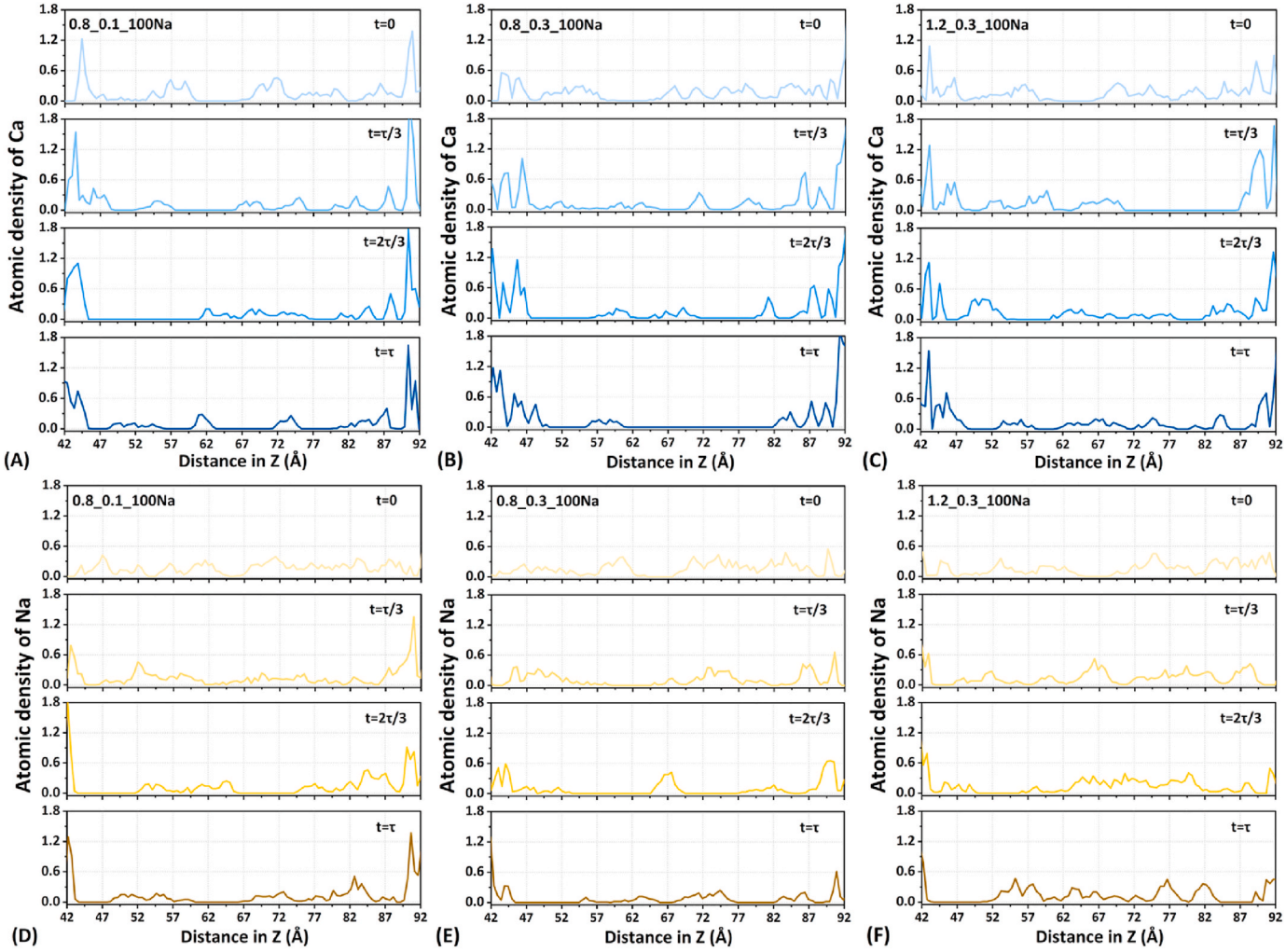

Fig. A1. Atomic density profiles of Ca and Na ions along the Z-axis of 5 nm nanopore (from 42 to 92 Å) perpendicular to the surface of the gels of "0.8_0.1_100Na", "0.8_0.3_100Na" and "1.2_0.3_100Na". τ is the total simulation time. In each inset, the locations near 42 Å and 92 Å at the "distance in Z" correspond to the gel substrates while that at around 67 Å is considered the centre of the nanopore of gels.

Fig. A2 shows the diffusion coefficient distribution of K at different positions along the Z-axis of the nanopore of the two C-(N,K-)A-S-H gels. Similar to Ca and Na, the diffusion coefficient of K near the gel substrate is lower than that in the centre of the nanopore. Based on Fig. A2, the average diffusion coefficient of K in gels 0.8_0.3_50Na50K and 0.8_0.3_10Na90K is calculated to be 1.37×10^{-9} m^2/s and 1.4×10^{-9} m^2/s, respectively, which is higher than that of Ca and Na.

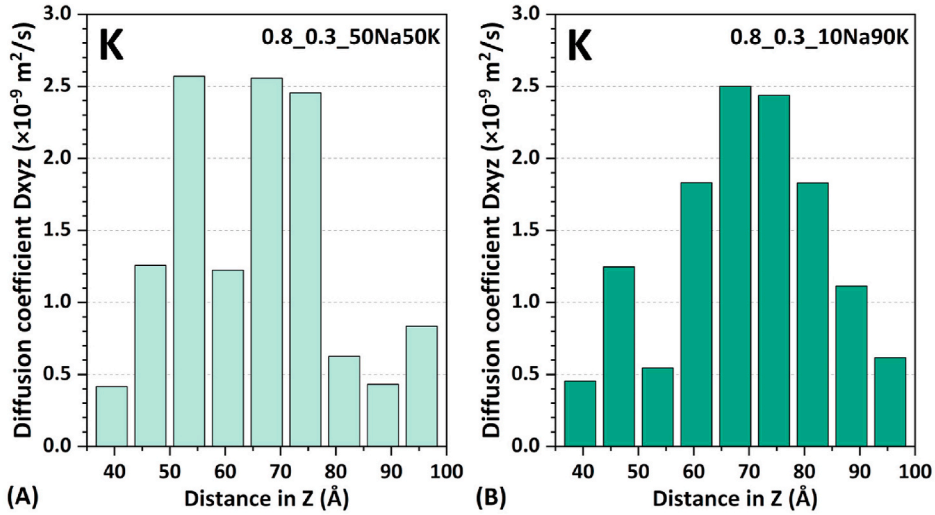

Fig. A2. Diffusion coefficient distributions of K along the Z-axis of the nanopore solution perpendicular to the surface of the two C-(N,K-)A-S-H gels.

Fig. A3 shows the radial distribution function (RDF, g(r))(solid lines) and the coordination numbers (dashed lines) of Na and K ions with water molecules. As implied by the X-axis value of the peak of g(r), the average bond length of K (~2.85 Å) is significantly higher than that of Na (~2.35 Å). According to the cutting distance of the RDF of Na (~3.6 Å) and K (~3.0 Å), the coordination numbers of Na and K with hydrated water molecules (obtained from the integral of g(r)) are 6 and 8, respectively.

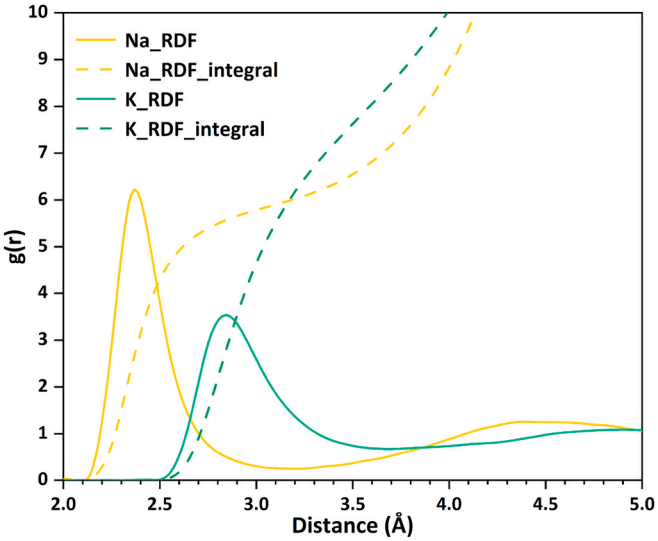

Fig. A3. Radial distribution function (solid lines) and the coordination numbers (dashed lines) of Na and K ions with O_W in water molecules.

The ClayFF assigns different charges to oxygen ions in hydroxyl groups based on their local bonding environment, as illustrated in Table A1. The charge of non-bridging oxygen in aluminosilicate chains is variable to maintain charge neutrality for different C-(N,K-)A-S-H gels.

Table A1
Atomic charge parameters in ClayFF simulations.

Atom type	Element type	Charge (e)	Description
Cao	Ca	1.36	Intralayer calcium in C-(N,K-)A-S-H gels
Ca	Ca	2	Interlayer calcium and aqueous Ca
St	Si	2.1	Silicon atoms in C-(N,K-)A-S-H gels
At	Al	1.575	Aluminium atoms in C-(N,K-)A-S-H gels
Na	Na	1	Sodium ions
K	K	1	Potassium ions
Hw	H	0.41	Hydrogen atoms in water
Ho	H	0.425	Hydrogen atoms in hydroxyl groups
Ow	O	-0.82	Oxygen atoms in water
Oh	O	-0.95	Oxygen atoms in free hydroxyl groups
Ohs	O	-1.0808	Hydroxyl O in aluminosilicate chains
Ob	O	-1.05	Bridging oxygen ions in aluminosilicate chains
Onb	O	-1.23 ~ -1.31	Non-bridging oxygen in aluminosilicate chains

Data availability

Data will be made available on request.

References

[1] Bullard JW, Jennings HM, Livingston RA, Nonat A, Scherer GW, Schweitzer JS, Scrivener KL, Thomas JJ. Mechanisms of cement hydration. Cement Concr Res 2011;41:1208–23. https://doi.org/10.1016/j.cemconres.2010.09.011.

[2] Snellings R, Suraneni P, Skibsted J. Future and emerging supplementary cementitious materials. Cement Concr Res 2023;171. https://doi.org/10.1016/j.cemconres.2023.107199.

[3] Kasaniya M, Thomas MDA. Role of the alkalis of supplementary cementing materials in controlling pore solution chemistry and alkali-silica reaction. Cement Concr Res 2022;162:107007. https://doi.org/10.1016/j.cemconres.2022.107007.

[4] Feng L, Yi S, Zhao S, Zhong Q, Ren F, Liu C, Zhang Y, Wang W, Xie N, Li Z, Cui N. Recycling of aluminosilicate-based solid wastes through alkali-activation: preparation, characterization, and challenges. Buildings 2024;14. https://doi.org/10.3390/buildings14010226.

[5] Ouellet-Plamondon C, Habert G. Life cycle assessment (LCA) of alkali-activated cements and concretes. Woodhead Publishing Limited; 2015. https://doi.org/10.1533/9781782422884.5.663.

[6] Richardson IG, Brough AR, Groves GW, Dobson CM. The characterization of hardened alkali-activated blast-furnace slag pastes and the nature of the calcium silicate hydrate (C-S-H) phase. Cement Concr Res 1994;24:813–29. https://doi.org/10.1016/0008-8846(94)90002-7.

[7] Wang S-D, Scrivener KL. Hydration products of alkali activated slag cement. Cement Concr Res 1995;25:561–71. https://doi.org/10.1016/0008-8846(95)00045-E.

[8] Myers RJ, Bernal SA, Gehman JD, Van Deventer JSJ, Provis JL. The role of al in cross-linking of alkali-Activated slag cements. J Am Ceram Soc 2015;98:996–1004. https://doi.org/10.1111/jace.13360.

[9] Myers RJ, Bernal SA, San Nicolas R, Provis JL. Generalized structural description of calcium-sodium aluminosilicate hydrate gels: the cross-linked substituted tobermorite model. Langmuir 2013;29:5294–306. https://doi.org/10.1021/la4000473.

[10] Özçelik VO, White CE. Nanoscale charge-balancing mechanism in alkali-substituted calcium-silicate-hydrate gels. J Phys Chem Lett 2016;7:5266–72. https://doi.org/10.1021/acs.jpclett.6b02233.

[11] Myers RJ, L'Hôpital E, Provis JL, Lothenbach B. Composition-solubility-structure relationships in calcium (alkali) aluminosilicate hydrate (C-(N,K-)A-S-H). Dalton Trans (2003) 2015;44:13530–44. https://doi.org/10.1039/c5dt01124h.

[12] Garcia-Lodeiro I, Palomo A, Fernández-Jiménez A, MacPhee DE. Compatibility studies between N-A-S-H and C-A-S-H gels. Study in the ternary diagram Na2O-CaO-Al2O3-SiO 2-H2O. Cement Concr Res 2011;41:923–31. https://doi.org/10.1016/j.cemconres.2011.05.006.

[13] Wang Y, Cao Y, Zhang Z, Huang J, Zhang P, Ma Y, Wang H. Study of acidic degradation of alkali-activated materials using synthetic C-(N)-A-S-H and N-A-S-H gels. Composites Part B 2021;230:109510. https://doi.org/10.1016/j.compositesb.2021.109510.

[14] Liu C, Li Z, Nie S, Skibsted S, Ye G. Structural evolution of calcium sodium aluminosilicate hydrate (C-(N-)A-S-H) gels induced by water exposure: the impact of Na leaching. Cement Concr Res 2024;178. https://doi.org/10.1016/j.cemconres.2024.107432.

[15] Duque-Redondo E, Bonnaud PA, Manzano H. A comprehensive review of C-S-H empirical and computational models, their applications, and practical aspects. Cement Concr Res 2022;156:106784. https://doi.org/10.1016/j.cemconres.2022.106784.

[16] Zuo Y, Chen Y, Liu C, Gan Y, Göbel L, Ye G, Provis JL. Modeling and simulation of alkali-activated materials (AAMs): a critical review. Cement Concr Res 2025;189. https://doi.org/10.1016/j.cemconres.2024.107769.

[17] Abdolhosseini Qomi MJ, Ulm FJ, Pellenq RJM. Evidence on the dual nature of aluminum in the calcium-silicate-hydrates based on atomistic simulations. J Am Ceram Soc 2012;95:1128–37. https://doi.org/10.1111/j.1551-2916.2011.05058.x.

[18] Churakov SV, Labbez C. Thermodynamics and molecular mechanism of Al incorporation in calcium silicate hydrates. J Phys Chem C 2017;121:4412–9. https://doi.org/10.1021/acs.jpcc.6b12850.

[19] Yang J, Hou D, Ding Q. Structure, dynamics, and mechanical properties of cross-linked calcium aluminosilicate hydrate: a molecular dynamics study. ACS Sustainable Chem Eng 2018;6:9403–17. https://doi.org/10.1021/acssuschemeng.8b01749.

[20] Hou D, Li T. Influence of aluminates on the structure and dynamics of water and ions in the nanometer channel of calcium silicate hydrate (C-S-H) gel. Phys Chem Chem Phys 2018;20:2373–87. https://doi.org/10.1039/c7cp06985e.

[21] Hou D, Li T, Wang P. Molecular dynamics study on the structure and dynamics of NaCl solution transport in the nanometer channel of CASH gel. ACS Sustainable Chem Eng 2018;6:9498–509. https://doi.org/10.1021/acssuschemeng.8b02126.

[22] Tao Y, Gao Y, Sun Y, Pellenq RJM, Poon CS. C-S-H decalcification in seawater: the view from the nanoscale. Cement Concr Res 2024;175:107385. https://doi.org/10.1016/j.cemconres.2023.107385.

[23] Liu C, Liang X, Chen Y, Li Z, Ye G. Degradation of alkali-activated slag subject to water immersion. Cem Concr Compos 2022;142. https://doi.org/10.1016/j.cemconcomp.2023.105157.

[24] Liu C, Zhang Y, Liang M, Li Z, Ye G. Underwater carbonation of alkali-activated slag pastes. Constr Build Mater 2024;445:137967. https://doi.org/10.1016/j.conbuildmat.2024.137967.

[25] Liu C, Haoming W, Zhenming L, Hu S, Guang Y. Effect of curing condition on mechanical properties and durability of alkali-activated slag mortar. Constr Build Mater 2024;439:137376. https://doi.org/10.1016/j.conbuildmat.2024.137376.

[26] Liu C, Li Z, Ye G. Mechanisms of efflorescence of alkali-activated slag. Cem Concr Compos 2025;155:105811. https://doi.org/10.1016/j.cemconcomp.2024.105811.

[27] Zhang Z, Provis JL, Ma X, Reid A, Wang H. Efflorescence and subflorescence induced microstructural and mechanical evolution in fly ash-based geopolymers. Cem Concr Compos 2018;92:165–77. https://doi.org/10.1016/j.cemconcomp.2018.06.010.

[28] Zhang Z, Provis JL, Reid A, Wang H. Fly ash-based geopolymers: the relationship between composition, pore structure and efflorescence. Cement Concr Res 2014;64:30–41. https://doi.org/10.1016/j.cemconres.2014.06.004.

[29] Martín-Garrido M, Teresa Molina-Delgado M, Martínez-Ramírez S. A comparison between experimental and theoretical Ca/Si ratios in C–S–H and C–S(A)–H gels. J Sol Gel Sci Technol 2020;94:11–21. https://doi.org/10.1007/s10971-019-05097-x.

[30] Gomez-Zamorano L, Balonis M, Erdemli B, Neithalath N, Sant G. C–(N)–S–H and N–A–S–H gels: compositions and solubility data at 25°C and 50°C. J Am Ceram Soc 2017;100:2700–11. https://doi.org/10.1111/jace.14715.

[31] L'Hôpital E, Lothenbach B, Le Saout G, Kulik D, Scrivener K. Incorporation of aluminium in calcium-silicate-hydrates. Cement Concr Res 2015;75:91–103. https://doi.org/10.1016/j.cemconres.2015.04.007.

[32] Yan Y, Yang SY, Miron GD, Collings IE, L'Hôpital E, Skibsted J, Winnefeld F, Scrivener K, Lothenbach B. Effect of alkali hydroxide on calcium silicate hydrate (C-S-H). Cement Concr Res 2022;151. https://doi.org/10.1016/j.cemconres.2021.106636.

[33] Van der Sloot HA, Kosson DS, Zomeren A. Landfilling of different kinds of waste: leaching behavior. Elsevier Inc.; 2018. https://doi.org/10.1016/B978-0-12-407721-8.00052-8.

[34] Zhang Y, Cetin B, Likos WJ, Edil TB. Impacts of pH on leaching potential of elements from MSW incineration fly ash. Fuel 2016;184:815–25. https://doi.org/10.1016/j.fuel.2016.07.089.

[35] Anderson JC, Dubetz C, Palace VP. Neonicotinoids in the Canadian aquatic environment: a literature review on current use products with a focus on fate, exposure, and biological effects. Sci Total Environ 2015;505:409–22. https://doi.org/10.1016/j.scitotenv.2014.09.090.

[36] D. Hou, Molecular simulation on cement-based materials, [n.d].

[37] Bonaccorsi E, Merlino S, Kampf AR. The crystal structure of tobermorite 14 Å (plombierite), a C–S–H phase. J Am Ceram Soc 2005;88:505–12.

[38] Abdolhosseini Qomi MJ, Krakowiak KJ, Bauchy M, Stewart KL, Shahsavari R, Jagannathan D, Brommer DB, Baronnet A, Buehler MJ, Yip S, Ulm FJ, Van Vliet KJ, Pellenq RJM. Combinatorial molecular optimization of cement hydrates. Nat Commun 2014;5:1–10. https://doi.org/10.1038/ncomms5960.

[39] Tao Y, Zare S, Wang F, Qomi MJA. Atomistic thermodynamics and kinetics of dicalcium silicate dissolution. Cement Concr Res 2022;157:106833. https://doi.org/10.1016/j.cemconres.2022.106833.

[40] Allen AJ, Thomas JJ, Jennings HM. Composition and density of nanoscale calcium-silicate-hydrate in cement. Nat Mater 2007;6:311–6. https://doi.org/10.1038/nmat1871.

[41] Plimpton S, Crozier P, Thompson A. LAMMPS-large-scale atomic/molecular massively parallel simulator. Sandia Natl. Lab. 2007;18:43.

[42] Beveridge DL, DiCapua FM. Free energy via molecular simulation: applications to chemical and biomolecular systems. Annu Rev Biophys Biophys Chem 1989;18:431–92. https://doi.org/10.1146/annurev.bb.18.060189.002243.

[43] Barducci A, Bonomi M, Parrinello M. Metadynamics. Wiley Interdiscip Rev Comput Mol Sci 2011;1:826–43. https://doi.org/10.1002/wcms.31.

[44] Kastner J. Umbrella sampling. Wiley Interdiscip Rev Comput Mol Sci 2011;1:932–42. https://doi.org/10.1002/wcms.66.

[45] Park S, Schulten K. Calculating potentials of mean force from steered molecular dynamics simulations. J Chem Phys 2004;120:5946–61. https://doi.org/10.1063/1.1651473.

[46] Barducci A, Bussi G, Parrinello M. Well-tempered metadynamics: a smoothly converging and tunable free-energy method. Phys Rev Lett 2008;100:20603.

[47] Laio A, Parrinello M. Escaping free-energy minima. Proc Natl Acad Sci USA 2002;99:12562–6.

[48] Bonomi M, Branduardi D, Bussi G, Camilloni C, Provasi D, Raiteri P, Donadio D, Marinelli F, Pietrucci F, Broglia RA. PLUMED: a portable plugin for free-energy calculations with molecular dynamics. Comput Phys Commun 2009;180:1961–72.

[49] Tao Y, Martin P, Manzano H, Qomi MJA. Mesoscopic mechanisms of dicalcium silicate dissolution. Cement Concr Res 2025;189. https://doi.org/10.1016/j.cemconres.2024.107660.

[50] Stranski IN. Zur theorie des kristallwachstums. Z Phys Chem (Leipz) 1928;136:259–78.

[51] Kossel W. Extending the law of bravais. Nachr. Ges. Wiss. Göttingen. 1927;143:135–43.

[52] Cygan RT, Liang J-J, Kalinichev AG. Molecular models of hydroxide, oxyhydroxide, and clay phases and the development of a general force field. J Phys Chem B 2004;108:1255–66.
[53] Grangeon S, Claret F, Linard Y, Chiaberge C. X-ray diffraction: a powerful tool to probe and understand the structure of nanocrystalline calcium silicate hydrates. Acta Crystallogr. Sect. B Struct. Sci. Cryst. Eng. Mater. 2013;69:465–73.
[54] Yang S. Sodium sites and hydration state in C − S − H phases synthesized under alkaline conditions from 1 H and 23 Na NMR experiments. J Phys Chem C 2024. https://doi.org/10.1021/acs.jpcc.4c01982.
[55] Yang SY, Yan Y, Lothenbach B, Skibsted J. Incorporation of sodium and aluminum in cementitious calcium-alumino-silicate-hydrate C-(A)-S-H phases studied by 23Na, 27Al, and 29Si MAS NMR spectroscopy. J Phys Chem C 2021;125:27975–95. https://doi.org/10.1021/acs.jpcc.1c08419.
[56] Duxson P, Lukey GC, Separovic F, Van Deventer JSJ. Effect of alkali cations on aluminum incorporation in geopolymeric gels. Ind Eng Chem Res 2005;44:832–9. https://doi.org/10.1021/ie0494216.
[57] Henkelman G, Uberuaga BP, Jónsson H. Climbing image nudged elastic band method for finding saddle points and minimum energy paths. J Chem Phys 2000; 113:9901–4. https://doi.org/10.1063/1.1329672.
[58] Diamond S, Dolch WL, White JL. Studies on tobermorite-like calcium silicate hydrates. Highw Res Rec 1964.
[59] Pellenq RJ, Caillol JM, Delville A. Electrostatic attraction between two charged surfaces : a (N , V , T). Monte Carlo Simulation 1997;5647:8584–94.
[60] Mills R, Lobo VMM. Self-diffusion in electrolyte solutions: a critical examination of data compiled from the literature. Elsevier; 2013.
[61] Li Z, Merz KM. Systematic evaluation of ion diffusion and water exchange. J Chem Theor Comput 2021. https://doi.org/10.1021/acs.jctc.1c01189.
[62] Sposito G. The chemistry of soils. Oxford university press; 2008.
[63] Atkins P, Atkins PW, de Paula J. Atkins' physical chemistry. Oxford university press; 2014.
[64] Polte J. Fundamental growth principles of colloidal metal nanoparticles–a new perspective. CrystEngComm 2015;17:6809–30.
[65] Helmholtz H. Ueber einige Gesetze der Vertheilung elektrischer Ströme in körperlichen Leitern mit Anwendung auf die thierisch-elektrischen Versuche. Ann Phys 1853;165:211–33. https://doi.org/10.1002/andp.18531650603.
[66] Atkins PW, De Paula J, Keeler J. Physical chemistry. Oxford university press; 1998.
[67] Visser JHM. Fundamentals of alkali-silica gel formation and swelling: condensation under influence of dissolved salts. Cement Concr Res 2018;105:18–30. https://doi.org/10.1016/j.cemconres.2017.11.006.
[68] Snelders HAM. De geschiedenis van de scheikunde in Nederland. Deel; 2008.
[69] Tänzer R, Jin Y, Stephan D. Alkali activated slag binder: effect of cations from silicate activators. Mater. Struct. Constr. 2017;50. https://doi.org/10.1617/s11527-016-0961-y.
[70] Tänzer R, Buchwald A, Stephan D. Effect of slag chemistry on the hydration of alkali-activated blast-furnace slag. Mater. Struct. Constr. 2014;48:629–41. https://doi.org/10.1617/s11527-014-0461-x.